OPEN ACCESS
IOP Publishing
Journal of Physics D: Applied Physics
J. Phys. D: Appl. Phys. **48** (2015) 363001 (28pp)
doi:10.1088/0022-3727/48/36/363001

Topical Review

Quantum dot optoelectronic devices: lasers, photodetectors and solar cells

Jiang Wu, Siming Chen, Alwyn Seeds and Huiyun Liu

Department of Electronic and Electrical Engineering, University College London, Torrington Place, London WC1E 7JE, UK

E-mail: huiyun.liu@ucl.ac.uk

Received 27 January 2015
Accepted for publication 23 April 2015
Published 17 August 2015

Abstract

Nanometre-scale semiconductor devices have been envisioned as next-generation technologies with high integration and functionality. Quantum dots, or the so-called 'artificial atoms', exhibit unique properties due to their quantum confinement in all 3D. These unique properties have brought to light the great potential of quantum dots in optoelectronic applications. Numerous efforts worldwide have been devoted to these promising nanomaterials for next-generation optoelectronic devices, such as lasers, photodetectors, amplifiers, and solar cells, with the emphasis on improving performance and functionality. Through the development in optoelectronic devices based on quantum dots over the last two decades, quantum dot devices with exceptional performance surpassing previous devices are evidenced. This review describes recent developments in quantum dot optoelectronic devices over the last few years. The paper will highlight the major progress made in 1.3 μm quantum dot lasers, quantum dot infrared photodetectors, and quantum dot solar cells.

Keywords: quantum dots, laser, detector and solar cells

(Some figures may appear in colour only in the online journal)

1. Introduction

Self-assembled nanostructures have been a subject of great interest and importance for several decades. Many unique properties, such as quantum effects, can be obtained by downscaling the dimensions of a semiconductor to nanoscale. As a result of the quantum size effect, the electrical and optical properties of nanometre-sized semiconductors can be engineered through controlling their morphology. Semiconductor quantum dots (QDs), analogous to atoms, represent an interesting nanoscale system with carriers confined in all dimensions. Unlike the traditional bulk semiconductors, the 0D semiconductor nanostructures show superior tuneability and sensitivity to external parameters. Moreover, the zero-dimensionality of QDs leads to the presence of discrete energy levels and density of states reduced to a set of delta functions. The fundamental advantages of low-dimensional semiconductors attracted much attention. This can be traced back to the 1970s when Dingle and Henry recognized that wavelength tuneability and threshold reduction can be realized in quantum structured semiconductor lasers [1], which were later theoretically proved by Asada *et al* and Arakawa *et al* in the 1980s [2, 3]. For many years following these pioneer works, the efforts devoted to QDs and their applications in devices were mainly theoretical studies due to the lack of feasible fabrication technique for QDs. It was not until the early 1990s that self-assembled QDs could be fabricated thanks to the significant advances in epitaxial growth techniques [4–6]. Once self-assembled QDs were successfully fabricated, laser diodes based on QDs were soon produced operating at 77 K [7]. The successful demonstration of self-assembled QDs and the first QD laser led to an intense worldwide effort to further develop control over QD growth and produce high-performance laser devices.

Most studies of self-assembled QDs are focused on the lattice-mismatched material systems, such as In(Ga)As/GaAs and InAs/InP. A common interpretation of the heteroepitaxial growth modes of thin films is based on thermodynamic arguments. The epitaxial growth is mainly governed by the sum of free enthalpies/energies of epilayer (σ_e), interface (σ_i) and substrate surface (σ_s), $\Delta\sigma = \sigma_e + \sigma_i - \sigma_s$ [4]. Based on this thermodynamic consideration, heteroepitaxial growth can proceed with three different modes: the Frank–Van der Merve mode ($\Delta\sigma < 0$), the Volmer–Weber mode ($\Delta\sigma > 0$), and Stranski–Krastanov (S–K) mode (the intermediate growth mode with a change of sign of $\Delta\sigma$). From a thermodynamic point of view, the buildup strain tends to introduce dislocations before film relaxation during heteroepitaxy of lattice mismatched materials [8]. However, the epitaxial growth generally deviated from the thermodynamic case is a non-equilibrium process. The adatoms are sufficiently mobile to allow dynamic strain relaxation during epitaxial growth and hence formation of defect-free coherent 3D islands [9, 10]. The possibility for obtaining high quality QDs was soon confirmed by many studies and the last two decades have witnessed the major success of growing QDs on lattice mismatched surfaces by the S–K growth mode. Self-assembled QDs with high crystal quality have been successfully grown by various growth techniques, including solid-state molecular-beam epitaxy (MBE) [11–13], gas source MBE [14, 15], metal-organic chemical vapour deposition [16, 17], chemical-beam epitaxy, and metal organic vapour phase epitaxy [18, 19]. Droplet epitaxy, initially proposed by Koguchi *et al*, has also attracted a lot of attention in acquiring high quality semiconductor nanostructures through self-assembly [5]. Droplet epitaxy is based on crystallization of metal droplets preformed on a substrate surface using an element from another group. This unique growth protocol makes droplet epitaxy a flexible technique for fabrication of semiconductor nanostructures by self-assembly and permits design and precise control of complex semiconductor structures at nanoscale, such as the capability to grow 3D quantum structures on both lattice-mismatched and lattice-matched substrates. During the last ten years, a rich spectrum of nanomaterials, including QDs, quantum rings, and nanoholes, have been fabricated by droplet epitaxy [20–25]. Droplet epitaxy is also attractive to create nanopatterns *in situ* for growth of complex nanostructures, such as QD molecules, nanowires, and strain-free QDs [26–29]. The flexibility and advances in self-assembly epitaxy render a high degree of freedom in fabricating high quality building blocks for advanced optoelectronic devices.

The progress made in self-assembly of QDs has soon paid off. In addition to lasers, optoelectronic devices, including quantum dot infrared photodetectors (QDIPs), quantum dot solar cells (QDSCs), quantum dot superluminescent diodes (QDSLDs), and quantum dot amplifiers have been reported. For example, in the late 1990s, the intersubband absorption in the QDs led to the development of mid-wavelength and long-wavelength infrared photodetectors [30, 31]. In 2000s, QDSCs, quantum dot amplifiers, and QDSLDs were also reported by several groups [32–36]. In order to fulfil the promise of high performance QD optoelectronic devices, the activities on improving the material growth and device design are still continuing. Although the developments of QD optoelectronic devices have been summarized separately in a few reports [37–41], in this paper, the recent rapid developments in the fields of QD lasers, QDSCs, and QDIPs are reviewed. The main text of this review consists of three sections. The first section discusses the progress made in QD lasers. The second section is focused on the developments of QDIPs. The third section reviews the recent advances of QDSCs. Finally, this paper closes with a summary of the progress of QD optoelectronic devices and the prospects and challenges for the future of the field.

2. Quantum dot lasers

2.1. Advantages of quantum dot lasers

Since the idea of using a double heterostructure as an active region of a semiconductor laser in 1963 [42, 43], quantum structured lasers have received much attention. In particular, the advances in epitaxial processes in the last 30 years made revolutionary developments possible in the field of semiconductor optoelectronic devices. The success of reducing the dimensionality of the active region from double heterostructure to quantum well (QW), quantum wire, and, in the ultimate case, quantum dot has soon drawn wide attention to quantum-confined laser structures. An immediate effect of using quantum heterostructures with additional degrees of quantization in lasers is to modify the density of states of electrons and holes. The 3D quantum confinement in QDs focuses the injected non-equilibrium carriers in a narrower energy range than that in bulk and QWs with 1D quantization, and thus, results in much steeper dependence of optical gain on the injection current, while the transparency current is reduced because of rapid filling of the charge carriers at the energy of the working transition and population inversion with fewer injected carriers [2]. Given the same homogeneous broadening, Asada *et al* theoretically demonstrated an increase of gain with increasing degree of quantum confinement and over one order of improvement in material gain in QDs compared to QWs. Material gain in QDs is expected to further increase with decreased physical size of QDs [2]. The high degree of quantization and discrete energy levels also account for the strong oscillator strength of the optical transitions per unit volume in QDs as a result of localization of electron and hole wave functions [44]. Moreover, due to a more symmetric gain function in QDs, linewidth enhancement factor, α-factor, as well as chirp for QD lasers can be much smaller in comparison to QW devices. A typical value of α for QD lasers is a few times lower than for QW lasers [45, 46]. Reduced inhomogeneous broadening of QDs can potentially lead to an α-factor as small as 0.1, which is of great importance for achieving high-modulation speed of lasers [47–49]. On the other hand, the atom-like energy levels of QDs have dramatically suppressed thermal spreading of the injected carriers as well as the relatively large energy separations between the lowest energy state and higher energy states, which can be thermally populated, which weakens the temperature dependence of QD lasers as predicted by Arakawa and Sakaki in 1982 [3]. In a practical QD laser structure, the

injected carriers can thermally escape from the lowest energy state, i.e. QD ground state, into the excited states, wetting layer, or even jump out of the heterostructures. As a result, the recombination processes of the thermalized carriers outside of QD ground states give rise to an additional component of the threshold current, which depends exponentially on temperature. Charge neutrality violation in QDs also brings in a temperature-dependent threshold current component of lasers [50]. Nevertheless, QD lasers exhibit great temperature stability compared with their QW and bulk counterparts. Large characteristic temperature (T_0) can be obtained by optimizing the QD assembly parameters and the device structure design [46]. In addition, the localization of charge carriers in QDs reduces nonradiative surface recombination, which decreases facet overheating and increases the threshold of catastrophic optical damage [51], and such an advantage allows fabrication of QD lasers with high output power. The advantages of QD lasers also include lower sensitivity to nonradiative recombination centres in or in the vicinity of the active region than the QW case, which is caused by a reduced interaction with the defects due to carrier localization in the QDs [52]. The QD array also prevents the movement of dislocations due to the presence of a strong strain field, and therefore QD lasers exhibit longer lifetime and superior reliability performance compared with QW devices, even in the presence of high-density nonradiative recombination centres [53].

Many of these basic advantages of QD lasers have been successfully demonstrated. However, self-assembly techniques inevitably lead to significant QD size fluctuations. The inhomogeneous broadening of self-assembled QDs deviates from the ideal QD structure, leading to a spreading of the gain over a wider spectral range, reducing the maximum peak gain. As a result, a much broader spectral linewidth is observed from QDs than QWs and the maximum gain is a strong function of the QD parameters, including QD density, the number of QD layers, QD morphology, as well as QD size distribution. In addition to the QD parameters, the laser structure, such as optical confinement layers, doping profile, and energy band profile, affect the characteristics of QD lasers [54]. Over the years, the optimization of self-assembled QDs as well as device structures has been the subject of continuous efforts, which led to the realization of QD lasers approaching the theoretical limits. Although QD have been successfully applied in lasers at different wavelengths, the telecommunication wavelengths at 1.31 and 1.55 μm are considered of the most importance. The lasers at telecommunication wavelengths based on self-assembled QDs have been well developed in the last 15 years and hold the promise for photonic integrated circuits. The recent developments of QD lasers, operating near 1.55 μm and at longer wavelengths, have been reviewed by Li *et al* [55]. In this section, a summary of the major milestones and the state-of-the-art of QD lasers recently developed are presented with a focus on 1.3 μm lasers.

2.2. Progress in quantum dot lasers

Since the first recognition of the fundamental advantages of QDs in laser applications [1], it has taken about two decades for the experimental realization of the first QD laser by Hirayama *et al* [56]. The QD laser was fabricated by wet etching of a layer of tensile strained QW into quantum boxes followed by regrowth. Lasing via excited states was obtained at a threshold current density as high as 7.6 kA cm^{-2} under pulse mode at 77 K, which is over one order of magnitude higher than the threshold of the QW laser fabricated from the same wafer measured under CW mode at room temperature. At almost the same time, Kirstaedter *et al* reported the first laser based on self-assembled QDs in 1994 showing lasing via the ground states with low threshold and large T_0 [7]. However, the good performance of the QD laser was limited to low temperature operation and a high threshold current density of 950 A cm^{-2} was measured at room temperature. Even so, this breakthrough inspired many later studies and initiated rapid improvements in the field of QD lasers. In a few years, the threshold current density of QD lasers has surpassed the best value for QW lasers that have been developed for a couple of decades, as shown in figure 1. It is only two years after the first demonstration of self-assembled QD lasers that a laser based on vertically coupled QDs with a low threshold (60 A cm^{-2}) has been realized, which was comparable to the lowest previously reported threshold for QWs [57]. After another two years, the first 1.3 μm QD laser was reported by Huffaker *et al* in 1998 [58]. In this work, a single layer of $In_{0.5}Ga_{0.5}As$ QDs was used to achieve near 1.3 μm lasing from ridge waveguide broad-area laser with high-reflectivity coating and a relatively low threshold current density of 270 A cm^{-2} at room temperature. In 1999, a dot-in-a-well (DWELL) structure has been used by Liu *et al* to obtain near 1.3 μm emission and an area density as high as 7×10^{10} cm^{-2} [59]. An extremely low threshold current density of 26 A cm^{-2} has been achieved under pulse mode at room temperature for a broad area QD laser (100 μm $\times$ 7.8 mm) with uncoated cleaved-facets. This value is nearly half of the best-reported value of QW lasers. In the same year, Mukai *et al* (DWELL, three layers) and Park *et al* ($In_{0.5}Ga_{0.5}As$ QDs, single layer) reported low threshold current densities of 200 A cm^{-2} and 45 A cm^{-2}, respectively, under continuous-wave (CW) operation with HR coating [60, 61]. In 2000, Huang *et al* reported a very low threshold current density CW 1.3 μm lasing of 32.5 A cm^{-2} (DWELL, single layer) and 25 A cm^{-2} (DWELL, double layer) at room temperature using an Al-oxide current confined laser structure without HR coating [62, 63]. In addition, the oxide-confined QD laser has also shown a very low internal loss ($\alpha = 0.77$ cm^{-1}), high external efficiency ($\eta_e = 55\%$), and high temperature operation up to 100 °C [63]. By using similar oxide-confined 1.3 μm QD lasers ($In_{0.5}Ga_{0.5}As$ QDs, single layer) with HR coating, Park *et al* reported a record low threshold current density of 19 A m^{-2} at the time of publication [64]. Liu *et al* reported a high performance multilayer (>3 layers) 1.3 μm QD laser by optimizing the DWELL structure and introducing the use of a high-growth-temperature GaAs spacer layer (HGTSL) [65–67]. The incorporation of HGTSLs was found to reduce the internal optical loss significantly from 15 $\pm$ 2 cm^{-1} to 3.5 $\pm$ 2 cm^{-1} [68]. Without either HR coating or oxide-confined structure, the multilayer QD laser demonstrated excellent performance with a room temperature threshold of

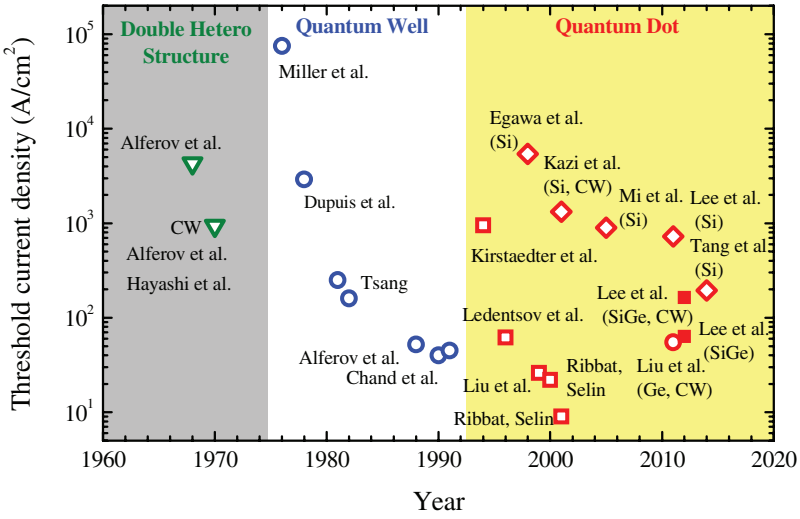

Figure 1. The historical development of heterostructure lasers showing the record threshold current densities at the time of publication (□ QD laser on GaAs; ■ QD laser on Ge; ○ QD laser on SiGe; ◆ QD laser on Si.) CW indicates that the threshold current values were obtained from QD lasers under continuous operation. The rest were obtained from QD lasers tested in pulse mode.

~30 A cm^{-2} and operating temperatures over 100 °C under both CW and pulse mode. Subsequently, by applying HR coating to the multilayer 1.3 μm QD laser, the authors demonstrated the lowest threshold of 17 A cm^{-2} (only ~5.7 A cm^{-2} per QD layer) at the time of publication [69, 70]. In 2008, Freisem *et al* reported a single layer QD laser (no HR coating) emitting at 1.22 μm with the lowest threshold current density (11.7 A cm^{-2}) ever reported previously for CW operation at room temperature [71]. This value was further reduced below 10 A cm^{-2} and at the same time a record low internal loss of 0.25 cm^{-1} was reported [72]. The low CW threshold current density obtained from QD laser demonstrates their promise in optical interconnects for minimizing power consumption and avoiding overheating of the lasers and adjacent electronic circuits.

Although very low threshold current densities of 1.3 μm QD lasers have been achieved by many groups within only a couple of years, these early devices did not show the good temperature stability expected. For example, both Liu *et al* and Park *et al* showed characteristic temperatures below 60 K while laser operation above room temperature was limited as a result of thermal escape of carriers from the InGaAs QW or thermal excitation of carriers into excited energy levels [59, 73]. The characteristic temperature was as low as 27 K between 25 and 40 °C as reported by Mukai *et al*, which was attributed to nonradiative recombination through defects and/or impurities [61]. In addition to nonradiative recombination through defects, the population of excited states and the wetting layer also contributes considerably to the threshold current density of high-performance QD lasers [74]. By comparing QD lasers with and without an InGaAs overgrowth layer, Mukai found that the QD laser without the InGaAs capping layer showed an energy separation between ground state to continuum 45 meV higher than that with the capping [75]. QDs grown by low growth rate enabled near 1.3 μm lasing even for the sample without InGaAs capping layer and the deep potential well suppressed thermal excitation of carriers into the continuum. As a result, a high characteristic temperature of 120 K at room temperature was achieved from the QD laser without InGaAs capping layer, about twice higher than the laser with InGaAs capping layer. The energy separation between the ground and first excited states also plays a critical role in the temperature stability of QD laser threshold. Chen *et al* obtained an energy separation of 95 meV between the ground and first excited state, which was over 20 meV larger than the typical valve for QDs [76]. The large energy separation led to a high T_0 of 460 K from 280 K to 300 K and 126 K from 300 K to 325 K. An improvement in the temperature stability can also be expected with multilayer QD lasers because the modal gain was increased and thermal excitation of carriers from the ground states into higher levels was reduced [77].

A breakthrough in thermal stability was achieved by the use of modulated p-type doping in QD lasers, which largely relaxes the requirements for careful control of the QD growth. By using this technique, Shchekin and Deppe showed a high characteristic temperature to 161 K between 0 and 80 °C [78]. By filling the hole energy levels, the decrease in maximum gain of ground state caused by thermal broadening of hole distribution can be eliminated. As a result, the temperature dependence of maximum gain is mainly determined by the widely separated electron energy levels and a high characteristic temperature can be achieved. The advantages of p-type doping has been further explored by Smowton *et al* and Sandall *et al* [79, 80]. Incorporation of p-type dopant also demonstrated negligible increase in non-radiative recombination and improved modal gain as a function of transparency point, which resulted in a 65% reduction in threshold at 300 K [81]. The increase in the maximum gain above room temperature with p-type modulation doping also leads to ground-state lasing up to 167 °C [78]. Shchekin *et al* later demonstrated an impressive high T_0 over 200 K between 0 and 81 °C for a 1.3 μm QD laser which combined p-type modulation doping with multilayer QD active region [82, 83]. Negative T_0 above room temperature was also reported by Badcock *et al*

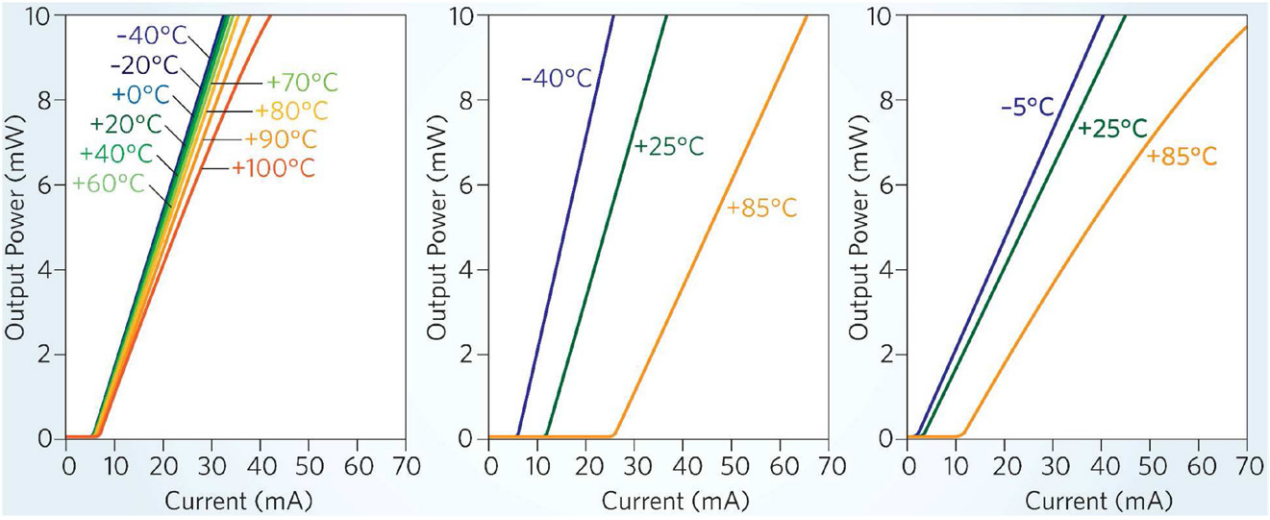

Figure 2. A comparison of typical power–current characteristics of FP lasers. The QD FP laser (left) provides temperature-insensitive operation with almost constant threshold current and slope efficiency. The other two panels show characteristics for two typical conventional QW lasers. Reprinted by permission from Macmillan Publishers Ltd: Nat. Photon. [92], copyright 2009.

using this method [84–86]. The negative T_0 around room temperature in p-doped QD lasers was attributed to the change in injection level required to achieve a fixed gain [87, 88]. Nearly complete temperature insensitivity of the threshold current can be achieved above room temperature via further optimization [89–91]. Almost constant threshold current density up to 100 °C has been demonstrated. Figure 2 compares the typical power-current characteristics of QD and QW lasers showing superior temperature performance of QD lasers over QW lasers [92]. As shown in figure 2, not only the threshold current density but also the output power and differential efficiency remain nearly unchanged from −40 to 100 °C for QD lasers. On the contrary, the power-current characteristics of two conventional QW lasers plotted in figure 2 show obvious temperature instability even around room temperature. Commercially produced 1.3 μm QD lasers by QD Laser Inc. can now produce high temperature CW operation up to 220 °C, T_0 of 500 K, and 25 Gb s^{-1} direct modulation bandwidth [92–94].

Over the years, apart from the work mentioned above, numerous studies worldwide in the field have demonstrated significant progress in QD laser performance, in terms of threshold current density, output power, gain, reliability, lifetime and dynamic characteristics and so on. As a brief review, this paper does not intend to cover all the aspects and interested readers are referred to the recent review paper published by Zhukov *et al* [95]. In the following the recent progress made in the field of QD lasers integrated on silicon substrates is reviewed.

2.3. Development of quantum dot lasers on silicon substrates

Silicon-based integrated circuits (ICs) have become incredibly fast and complex over the last few decades. The increasing complexity and functionality in ICs demand high bandwidth input/output to keep pace with processor performance. The growing data communication requirements make it challenging to continue using copper interconnects. The rationale behind development of photonic devices integrated with ICs is the high bandwidth demand and energy-efficient operation of photonic devices [96]. The last few years have witnessed great advances in silicon photonics and most key optical components, such as modulators and photodetectors, with excellent performance, developed on silicon substrates [97, 98]. However, the development of silicon photonics has been hindered by the lack of efficient light sources on silicon and the need to develop practical electrically pumped lasers on a Si platform has become increasingly urgent [99]. Unfortunately, group IV materials, like Si and Ge, are inefficient light-emitting materials due to their indirect bandgap. Therefore, an efficient electrically pumped light source is considered the 'holy grail' of Si photonics. Many efforts, along with much progress made in developing novel approaches, have been devoted to fabricate efficient light emitters on Si in the last decade. For example, Si Raman lasers have successfully demonstrated CW operation at room temperature [100]. However, the requirement of an external optical pumping source limited the Raman lasers for practical applications [101]. Low-dimensional Si materials, such as nanoporous Si and Si nanocrystals have not yet been shown as a possible route to gain efficient emission [102]. The recent Ge lasers fabricated on Si substrate still face a number of challenges and practical issues, such as high optical loss [103].

Monolithic or heterogeneous integration of III–V semiconductors on Si platforms has attracted much attention and been demonstrated as an effective route to photonic integrated circuits in the last few years. Impressive lasers with high output power and CW operation over 100 °C have been demonstrated by heterogeneous integration of III–V QD lasers on Si substrates through wafer bonding technology [104, 105]. Continuous efforts are being made to develop and improve the yield and reliability for III–V/Si heterogeneous integration [106]. However, monolithic integration of III–V light

sources on Si is often considered as the favourable approach. The significant material dissimilarity between III–Vs and Si makes monolithic III–V/Si integration challenging. The lattice mismatch and difference in thermal expansion coefficient between the two materials tend to generate a high density of dislocations, which dramatically undermines the superior optical properties of III–Vs [107, 108]. The direct epitaxy of III–V on Si mainly needs to deal with three types of defects: anti-phase boundaries (APBs), threading dislocations (TDs) and micro-cracks.

(1) Anti-phase boundaries: there are two different atomic sublattices in III–V semiconductors. Direct epitaxial growth of III–V materials on Si and Ge surfaces may cause shift of sublattice and sheets of wrong nearest neighbour bonds or APB can occur. APBs are planar defects and act as nonradiative recombination centres, which degrade device performance.
(2) Micro-cracks: thermal stress caused by the mismatch in thermal expansion coefficient between III–V epilayers and Si substrate can form micro-cracks in the epilayer during cooling from growth temperature (>500 °C) to room temperature.
(3) Threading dislocations: the 4.1% (7.5%) lattice mismatch between GaAs (InP) and Si introduces large strain in the III–V epilayer. The relaxation of the strain during growth generates a high density of TDs, typically on the order of $10^{10}\,cm^{-2}$. TDs act as nonradiative recombination centres and promote dark line defects in the semiconductor lasers, hence reducing device efficiency and lifetime.

Thanks to the development of III–V/Si buffer techniques, the above-mentioned defects can be well coped with, to the extent that laser devices with high performance can be developed. As described in section 2.1, QDs also have good tolerance to defects due to the localization of carriers and prevention of dislocation movement. Therefore, self-assembled III–V QDs are emerging as a promising technique for practical III–V/Si integration. The progress in monolithic integration of 1.3 μm QD lasers on Si platforms will be reviewed here.

2.3.1. Quantum dot lasers grown directly on Si substrates. Direct III–V/Si integration has been pursued over 30 years [109, 110]. The marriage between the most used electronic material and one of the most important optoelectronic materials will undoubtedly revolutionize the current information technology. However, after years of development, the density of TDs in the III–V epilayers on Si substrates is still of order of magnitude of $10^6\,cm^{-2}$, which makes the monolithic integration of III–V optoelectronic devices on Si unpractical for electronic circuits. For example, continuous-wave QW lasers operated at room temperature were reported but with high threshold and life time only slightly over 10 h [111–114]. Sugo *et al* achieved good performance (CW operation over 2000 h at room temperature) via multiple QW lasers emitting at 1.54 μm on Si with a III–V buffer layer of 15 μm, which, however, poses great challenges for connecting Si and III–V elements by high-resolution lithography methods [115]. The growth of III–V QDs on Si surfaces has also been attempted for nearly 20 years and GaAs QD based light-emitting diodes (LED) were reported at room temperature based on droplet epitaxy [116, 117]. However, the QD density was below $10^8\,cm^{-2}$ and the output power of this QD LED was only about 10% of an AlGaAs/GaAs QW LED grown on Si substrate. Gérard *et al* and Lacombe *et al* reported InAs/GaAs QDs grown on Si by S–K mode can achieve high area density ($>10^{10}\,cm^{-2}$) but only PL emission was reported up to 300 K [118, 119]. Nevertheless, compared with QWs, optical properties of QDs have been found to be unaffected by the presence of high dislocation density [118]. Given that QDs are effectively less sensitive to TDs and the striking progress made in the field of QD lasers, direct epitaxy of III–V QD on Si substrates is promising to obtain efficient light sources for photonic integrated circuits.

In 1998, just two years after the first report of direct epitaxy of III–V QDs on Si substrates, Egawa *et al* reported the first QD laser directly grown on Si substrates by droplet epitaxy [120]. A 2.5 μm thick GaAs buffer was grown directly on 2° misoriented Si(1 0 0) substrates, which was further thermally cycled from 350 and 850 °C for five times. Despite a low QD density ($<10^8\,cm^{-2}$), the authors managed to achieve room temperature operation under pulsed conditions. The threshold current density of this GaAs/AlGaAs QD laser was as high as $5.4\,kA\,cm^{-2}$. Since then, very limited number of papers on lasers based on droplet epitaxy QDs have been published until very recently when high QD density and improved crystal quality are become less challenging [121]. One year later, Linder *et al* reported the first self-assembled S–K QD lasers monolithically grown on Si substrates [122]. A 4 μm thick GaAs buffer was grown on 2° misoriented Si(1 0 0) substrates with an initial 30 nm GaAs nucleation layer grown at a low temperature of 350 °C. Two thermal cycles between 300 and 780 °C, including 10 min annealing at 780 °C, were used to improve the crystal quality, but a high density of TDs can still be observed in the active region of the laser. Despite an extremely high density of QDs (~$1.2 \times 10^{11}\,cm^{-2}$), lasing with a high threshold density of $3.85\,kA\,cm^{-2}$ was reported only under pulse mode at 80 K. In 2001, Kazi *et al* reported the first $In_xGa_{1-x}As$ QD laser operating in CW mode at room temperature [123]. Similarly, Si(1 0 0) substrates with 2° off-cut towards the [0 1 1] direction was used to suppress formation of anti-phase domains (APDs). A relatively thin 1 μm GaAs buffer was grown directly on Si substrates. A 10 nm GaAs nucleation layer was deposited on the Si substrates at 400 °C and thermal cycling from 350 °C to 850 °C for five times during buffer growth was also adopted to improve the material quality. CW operation of an $In_{0.2}Ga_{0.8}As$ QD laser at room temperature was demonstrated with a relatively low threshold current density of $1.32\,kA\,cm^{-2}$, which is about half of the value of an $In_{0.1}Ga_{0.9}As$ QW laser. Impressively, ageing tests showed that QD lasers on Si substrates were much more reliable than their QW counterparts; as shown in figure 3, stable operation of the QD lasers was measured for up to 80 h, while the performance of the QW lasers rapidly degraded within 20 h at room temperature under the automatic power control condition [123]. Later, Mi *et al* reported $In_{0.5}Ga_{0.5}As$ quantum dot lasers with an $Al_{0.07}Ga_{0.93}As$ core

waveguide on Si(1 0 0) substrates with 4° offcut towards the [1 1 1] direction [124]. A relatively low threshold current density of 1.5 kA cm^{-2} under pulsed bias conditions was measured. A high T_0 of 103 K in the temperature range 5 –95 °C was also observed due to a better carrier confinement in the QDs by using the AlGaAs core waveguide. By modulation doping the laser device with 20 holes per dot, T_0 of 244 K in the temperature range 25–95 °C was achieved. By incorporating ten periods of InGaAs/GaAs QDs as dislocation filter layers, Mi *et al* and Yang *et al* further reduced the threshold current density to 900 A cm^{-2} [125, 126].

Following the successful demonstration of the high-performance QD lasers epitaxially grown Si substrates, the same research group showed monolithic integration of the QD lasers and QW modulators based quantum-confined Stark effect (QCSE) on Si substrates [127]. The integration was achieved by following steps: (1) growing a same QD laser structure; (2) defining regions for modulators by standard photolithography; (3) regrowth of QW modulators; (4) processing of the ridge waveguide coupled laser-modulator by standard photolithography and metallization; (5) deposition of antireflection coating on modulator facets; and (6) focus ion beam milling of coupling groove between lasers and modulators. The integrated devices had a coupling efficiency of above 20% and a modulation depth of ~45% (100%) at a bias of −3 V (−5 V). The authors also reported monolithic integration of InGaAs/GaAs QD lasers with hydrogenated amorphous silicon waveguides (a:Si-H) on silicon substrates [128]. A coupling coefficient of 22% was reported. The fabrication of the laser/waveguide integration was very similar to the fabrication of QD laser/QCSE-QW modulator integration, except that SiO_x/a:Si-H/SiO_x waveguides were deposited by plasma enhanced chemical vapour deposition instead of regrowth of QW modulators.

These studies demonstrated the great potential of QD lasers directly grown on silicon for optical interconnects. However, all of these reports have not yet demonstrated QD lasers at the important telecommunication wavelengths at 1.3 and 1.55 μm. The pursuit of 1.3 μm QD lasers on Si substrates was driven by the urgent need for Si-based lasers at 1.3 and 1.55 μm as well as the significant developments of 1.3 μm QD/GaAs lasers at about the same period of time. In 2008, Li *et al* reported room temperature emission at 1.3 μm of a DWELL structure grown on Si(1 0 0) substrates with 6° miscut towards [0 1 1] direction [129]. Although a high QD density of 7 × 10^{10} cm^{-2} was achieved, the emission was rather broad (FWHM = 57 meV at 300 K) and the emission intensity was eight times weaker than that of the reference QD sample grown on GaAs. In 2011, the first 1.3 μm QD laser directly integrated on Si substrates became available through optimization of the GaAs buffer [130]. Si(1 0 0) substrates with 4° miscut towards [0 1 1] was used in the study. It is found out that the growth temperature of GaAs nucleation layer plays a critical role in determining the material quality of the laser devices. When a nucleation layer of 30 nm GaAs was grown with a slow growth rate of 0.1 ML/s at the optimized temperature of the 400 °C, more defects are confined within 50 nm of GaAs/Si interface compared with the samples grown

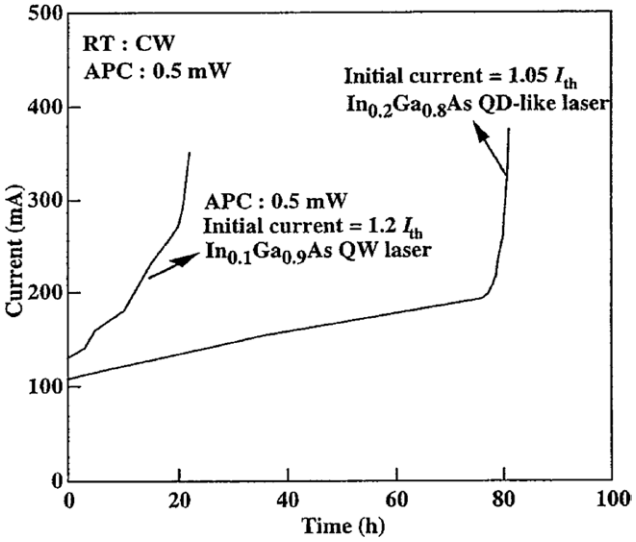

Figure 3. Reliability test of $In_{0.1}Ga_{0.9}As$ QW and $In_{0.2}Ga_{0.8}As$ QD lasers directly grown on Si substrates at room temperature under the automatic power control condition at a fixed output power of 0.5 mW. The initial current was set to be 1.2 times and 1.05 times of the threshold currents for QW and QD lasers, respectively. APC in the image stands for automatic power control. Reprinted with permission from [123]. Copyright 2001, AIP Publishing LLC.

at unoptimized nucleation temperatures. In addition to the 1-μm GaAs buffer, strained InGaAs/GaAs superlattices were used as dislocation filter layers to reduce the number of TDs propagating into the device active region. The laser consisted of five layers of DWELLs that were sandwiched between 1.5 μm $Al_{0.4}Ga_{0.6}As$ p and n-type cladding layers. Room temperature lasing at 1.3 μm was achieved with a low threshold current density of 725 A cm^{-2} for QD lasers directly grown Si substrates. Further reduction of the threshold current density to 650 A cm^{-2} was made possible by initializing the growth with an AlAs nucleation layer [131]. Compared with the GaAs nucleation layer, AlAs nucleation layer confined more defects at the III–V/Si interface and reduced the defect density by half. Recently, near room temperature CW operation of 1.3 μm QD lasers directly grown on Si substrates was demonstrated. Both the nucleation temperature and the thickness of the initial GaAs layer are optimized at low growth temperatures to reduce dislocation density. As a result, a low threshold current density of 458 A cm^{-2} under CW bias conditions was achieved at ~280 K [132]. However, the performance of these QD lasers on Si was still much inferior to those reported on GaAs substrates. Although an optimized nucleation layer can reduce the number of dislocations to some extent, the density of TDs can be still as high as ~10^9 cm^{-2}. Such a high dislocation density requires more effective dislocation filter layers. We have shown that TD density can be reduced to the order of ~10^5 cm^{-2} by improving the motion of TDs with misfit strain [133]. The key to obtain an effective dislocation filter structure is to maximize the amount of strain relaxed while keeping it within the critical value for dislocation multiplication. Indeed, by simply replace the InGaAs/GaAs strained-layer superlattices (SLSs) by InAlAs/GaAs SLSs, the density of threading dislocations was effectively reduced down to ~10^6 cm^{-2} [134].

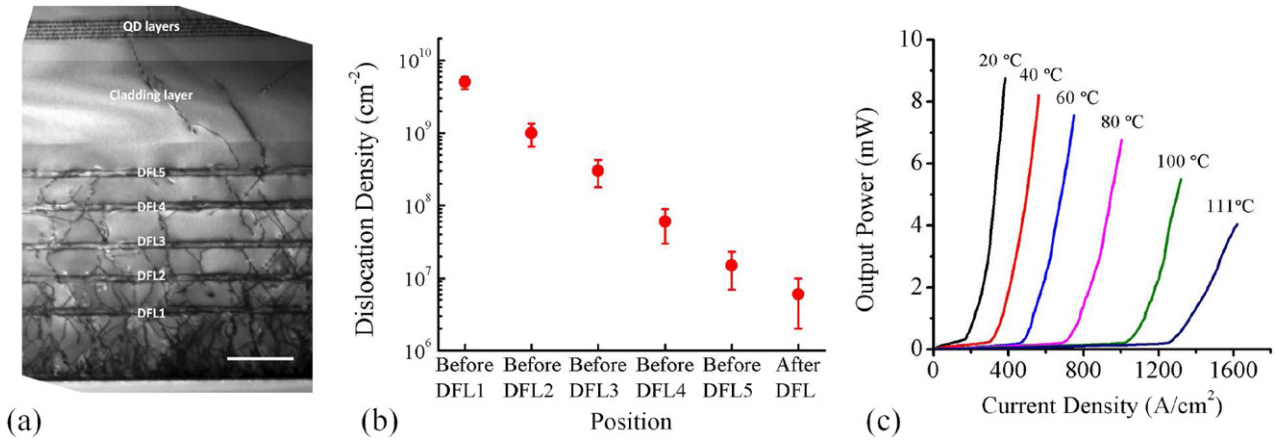

Figure 4. (a) Cross-sectional TEM image of a QD laser monolithically grown on offcut Si (1 0 0) substrates. DFL in the image stands for dislocation filter layers. The scale bar is 1 μm. (b) Dislocation density at different positions, determined by TEM. (c) Light output against current density for the QD laser at various temperatures [135].

A typical cross-sectional TEM image of QD lasers on Si was shown in figure 4(a). With five sets of dislocation filter layers, very low density of TDs can propagate into the active region. Figure 4(b) plotted dislocation density measured at different positions in the buffer of a QD laser grown on Si substrate. Each dislocation filter layer can effectively reduce the dislocation density by a few times and in the device active region, the dislocation density was reaching below $5 \times 10^6\,\mathrm{cm}^{-2}$. The improved effectiveness of dislocation filtering of InAlAs/GaAs SLSs was confirmed by etch pit density and photoluminescence measurements over a large area. Such a low density of TDs led to high performance QD lasers directly grown on Si substrates with an extremely low threshold current density of $194\,\mathrm{A\,cm}^{-2}$ and high output power of ~77 mW at room temperature. Lasing operation up to 85 °C has been measured for the as-cleaved broad-area lasers. Using the same method, as shown in figure 4(c), low-threshold current density of $200\,\mathrm{A\,cm}^{-2}$, high single facet output power over 100 mW and lasing operation up to 111 °C (limited by instrument constraints) have been achieved from uncoated 1.3 μm QD lasers directly grown on Si substrates [135]. It should be noted that these high-performance QD lasers grown on Si substrates were not thermally cycled as was done for early III–V lasers on Si. By using techniques such as multiple thermal cycling, p-type modulation doping, as well as facet coating, QD lasers on Si substrates are expected to achieve even better performance and are very promising for reaching the specifications required by photonic integrated circuits in the future.

2.3.2. Quantum dot lasers grown on Ge and Ge-on-Si substrates. In addition to direct growth of QD lasers on Si substrates, recent research efforts have also been directed to Ge virtual substrates. Compared with GaAs directly grown on Si, the lattice mismatch and thermal expansion coefficient mismatch between Ge and GaAs is much smaller. The lattice constant between Ge and GaAs is nearly the same with only 0.08% mismatch. The higher carrier mobilities and higher absorption coefficient in the optical communication wavelength region make Ge a good candidate for both electronics and optoelectronics. More importantly, Ge is compatible with silicon technology and Ge, and/or SiGe, based CMOS are very attractive for the sub-22 nm nodes [136]. Actually, the use of Ge layers as an interlayer for growth of III–V materials on Si substrates can be traced back to the early 1980s [137, 138]. However, it is only recently that Ge virtual substrates have gained renewed interests for III–V/Si integration as high quality and large scale Ge virtual substrates became available [136, 139]. In 2010, Bordel *et al* reported room temperature emission at 1.3 μm from QDs grown on germanium-on-insulator-on-silicon (GeOI) substrates with comparable intensity for QDs on GaAs substrates. The authors found that a single layer of QDs in the GaAs buffer was rather effective to reduce APDs. However, the insertion of QDs, even for multiple layers up to 10, had little impact on TDs and no laser was reported.

A breakthrough has been made by Liu *et al* in 2011, who did not only report the first 1.3 μm laser grown on a Ge substrate but also presented impressive device performance [140]. In this work, a Ga prelayer was introduced to suppress the formation of APDs and much improved material surface roughness was measured by AFM, as shown in figures 5(a) and (b). TEM measurements confirmed that the improved material quality was due to suppressed formation of APDs with use of the Ga prelayer, as shown in figures 5(c) and (d). Room temperature lasing at 1.305 μm was demonstrated by using five InAs/InGaAs DWELL layers under CW bias conditions. Despite the relative short history of development, an extremely low threshold current density of $55.2\,\mathrm{A\,cm}^{-2}$ (~$11\,\mathrm{A\,cm}^{-2}$ per dot layer) was achieved, which is comparable to the best previously reported values for QD lasers on GaAs and better than the state-of-the-art 1.3 μm InAs/GaAs QD lasers bonded on Si substrates (threshold current density of $205\,\mathrm{A\,cm}^{-2}$ for a laser with 10 layers of QDs) [66, 107]. The ultralow threshold along with high temperature CW operation (60 °C) provided an essential step towards the monolithic integration of III–V QD devices on Si substrates (figure 5(e)). Similarly to direct epitaxy of III–Vs on Si substrates, the initial nucleation layer also plays a critical role in the structural and optical properties of III–V materials on Ge substrates [141]. With an optimized GaAs nucleation layer, the authors obtained PL emission of QDs on Ge at 1.3 μm as strong as

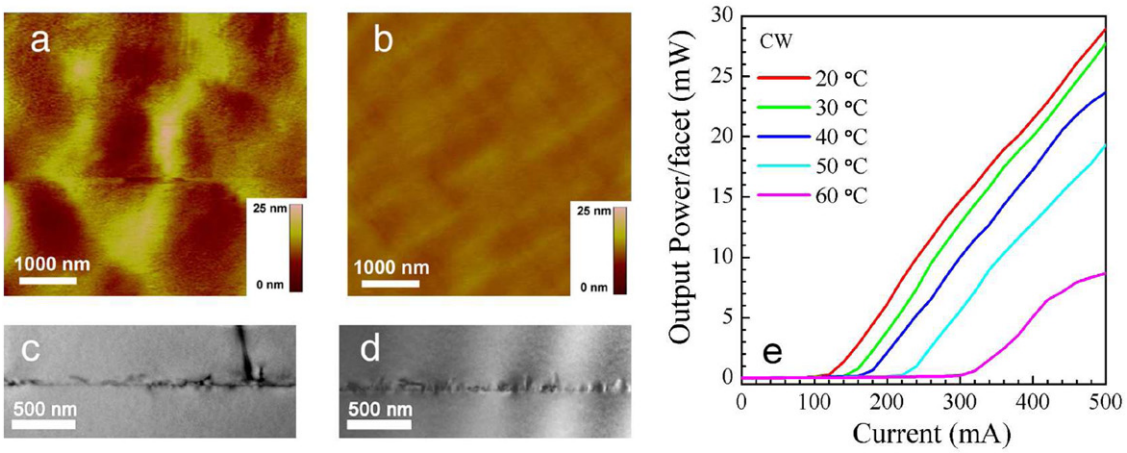

Figure 5. AFM images $5 \times 5\,\mu m^2$ of $1.2\,\mu m$ GaAs buffer layer grown on Ge substrates with (a) As prelayer and (b) Ga prelayer. TEM images of the interface between GaAs buffer layer and Ge substrate with (c) As prelayer and (d) Ga prelayer. (e) Light output against current for a five-layer InAs/GaAs QD laser at various heatsink temperatures. Reprinted by permission from Macmillan Publishers Ltd: Nat. Photon. [140], copyright 2011.

QDs on GaAs. A low room temperature threshold current density of $106\,A\,cm^{-2}$ and operation up to 100 °C were then demonstrated. These studies carried out at UCL have paved the way towards the monolithic integration of $1.3\,\mu m$ QD lasers on Si substrates through the use of Ge virtual substrates. Using the optimized growth procedures developed, in 2012, the first room temperature CW operation of Si-based QD lasers has been demonstrated [142]. The standard five-layer DWELL laser structure was grown on a Ge-on-Si substrate. The Ge virtual substrate was made by growing a $2\,\mu m$ p+ Ge layer using chemical vapour deposition (CVD) on Si(100) substrates with a 6° offcut towards the [1 1 1] direction. A very low threshold current density of $63.4\,A\,cm^{-2}$ ($163\,A\,cm^{-2}$) was achieved under pulse (CW) mode at room temperature, which is lower than the best-reported room temperature threshold current density values for III–V QD lasers on Si by bonding ($205\,A\,cm^{-2}$) and for III–V QW lasers on GeSi/Si by epitaxial growth ($269\,A\,cm^{-2}$) [107, 143]. Very recently, by using GaAs–Ge-on-Si virtual substrates, researchers from UCSB reported near $1.3\,\mu m$ QD lasers with exceptional high temperature performance approaching the state-of-the-art of QD lasers on GaAs substrates [144, 145]. The GaAs–Ge-on-Si virtual substrates consisted of 500 nm Ge grown by CVD and $1\,\mu m$ GaAs grown by MBE on Si(1 0 0) substrates with a 6° miscut towards the [1 1 1] direction. A dislocation density of $\sim 10^8\,cm^{-2}$ was presented in the GaAs layer of the virtual substrates. Over the GaAs–Ge-on-Si virtual substrates was grown a $2\,\mu m$ thick GaAs buffer followed by a typical GaAs/AlGaAs graded index separate confinement heterostructures waveguide laser structure with seven layers of DWELLs. Without any additional dislocation reduction layers or HR coatings, CW lasing at $1.25\,\mu m$ up to 95 °C and a high T_0 of 75 K measured between 20 and 60 °C were demonstrated for a p-type modulation doped QD laser [145]. After applying HR coating, the authors reported CW lasing up to 119 °C, low threshold of $427\,A\,cm^{-2}$, high output power of 176 mW, and high T_0 over 200 K [144, 145]. The development of QD lasers on group IV substrates showing record threshold-current densities as a function of publication year is also plotted in figure 1.

In addition to QD lasers, QD photodetectors, modulators, and superluminescent diodes with good performance have been reported on group IV substrates by direct epitaxy [146–149]. Based on these research efforts and rapid development in this field, monolithically integrated photonic circuits incorporating high performance III–V devices can be expected in the near future.

3. Quantum dot photodetectors

Quantum structured detectors have been intensively studied with the aim of creating the third-generation infrared detectors. Since the first report of intersublevel of transitions in quantum structures [150, 151], great progress has been made in the development of a variety of novel quantum structured photodetectors with improved performance. In 1998, thanks to the rapid developments in self-assembled QDs, Pan *et al* reported the first QDIP based on intersublevel transitions about the same time as the demonstration of the first QD laser [31].

QDIPs are operated in a similar manner as QW infrared photodetectors (QWIPs). The only difference is that the carriers in a QDIP are confined in all 3D instead of 1D. The 3D confinement of carriers in QDs provides many unique properties of QDIPs. For example, unlike QWIPs, QDIPs have high radiation tolerance due to localization of carriers, which is advantageous for space applications [152]. The major advantages of QDIPs over QWIPs can be summarized as follows [153]:

(1) QDIPs are intrinsically sensitive to infrared irradiation at normal incidence due to the breaking of the polarization selection rule [154]. Although p-type QWIPs are also capable of detecting normal incident light [155], the absorption, photoconductive gain, and responsivity are much lower due to the large hole effective mass and low hole mobility [156].
(2) QDIPs have lower dark current than QWIPs because of weaker thermionic emission from the QDs with 3D quantum confinement of carriers [157].

(3) The discrete energy levels in QDs have energy separations larger than that of the phonons, which reduce the phonon scattering and can lead to longer carrier lifetime (>100 ps) and higher operating temperature [158, 159].

However, QDIPs generally have a low quantum efficiency due to the small area fill factor of QDs and the limited number of QD layers [160, 161]. Another main disadvantage of QDIPs is the relatively large inhomogeneous broadening of the self-assembled QDs, which reduces absorption coefficient [162, 163]. Therefore, for the last 15 years, the growth and the design of novel QD heterostructures have been the centre of research efforts to realize the state-of-the-art QDIPs. In this section, the major advances in the field of QDIPs will be reviewed.

3.1. Towards high-performance quantum dot infrared photodetectors

Since the development of the first QDIP, a variety of material systems have been explored for high-performance QDIPs, including InAs/AlGaAs, InAs/InAlAs, In(Ga)As/GaAs, GaAs/AlGaAs and InGaAs/InGaP [154, 164–169]. Some of the approaches have demonstrated great potential to boost the performance of QDIPs. The research efforts to improve the QDIP performance can be mainly directed to two directions, reduction of noise or dark current and enhancement of responsivity. Although a low dark current is expected from QDIPs, the early devices showed similar or even higher dark currents compared with QWIPs. Such high dark currents can be attributed to populations of excited states and non-uniform doping in the QD region [170–172]. In order to reduce the dark current, Wang *et al* deposited a thin layer of AlGaAs immediately over InAs QDs [170, 171]. Due to the presence of QDs and strain distribution, the thickness of the AlGaAs layer was controlled to mainly cover the region without QDs. Despite the reduced carrier transport (hence lower responsivity) with the AlGaAs cap layer, the dark current of the QDIP with the AlGaAs layer was successfully reduced by three orders of magnitude and the detectivity was about 10 times higher than the reference device [170, 171]. Instead of using AlGaAs as a cap layer, Lin *et al* investigated the effects of using a single layer of $Al_{0.3}Ga_{0.7}As$ as a current blocking layer on either side of the QD active region, which showed both enhancement in responsibility and detectivity [164]. The improvement in responsivity was explained by the enhancement of the photoelectron avalanche process due to an increase of operation voltage while the current blocking layers suppressed the dark current. Simply by using the $Al_{0.3}Ga_{0.7}As$ current blocking layer on one side of the QD layers, superior temperature performance was also obtained and the background-limited performance reached from 125 to 175 K [164]. By using double $Al_{0.3}Ga_{0.7}As$ current blocking barriers outside of the QD region, the background-limited infrared photodetector (BLIP) of the QDIP was demonstrated to be as high as 250 K [173].

Doping in the active region also plays a critical role in the performance of QDIPs. Lee *et al* used delta doping of the AlGaAs barrier, which is 50 nm away from the QDs to create a high-mobility modulation-doped AlGaAs/GaAs heterointerfaces [174]. The high mobility channel improved the mobility of photoexcited carriers and led to a high photoconductive gain. As a result, a high responsivity of $4.7\,A\,W^{-1}$ and photosensitivity up to 190 K was observed [174]. On the other hand, Lin *et al* showed that direct doping of the QDs can lead to improved responsivity and lower dark current [175]. The improved responsivity with direct doping was attributed to the presence of a built-in electric field and the reduced dark current with direct doping was attributed to the increased activation energy [175]. Lee *et al* also showed that direct doping in the QDs can reduce the dark current. However, modulation doping in the GaAs barriers grown after QD formation may lead to a higher responsivity [175]. It is worth noting that satisfactory performance of doped QDIPs can only be expected with accurate control over growth conditions because growth defects introduced by dopants at high doping levels severely degrade the device performance [176, 177]. Attaluri *et al* also showed that there was an optimum doping level to obtain low dark current and high photocurrent [178]. Instead of modifying the doping profile in the active region, Wolde *et al* used a *p*-type structure with optical transition taking place in the valence band [179]. An immediate benefit would be an extended photoresponse into the THz wavelength range. The higher density of states and larger effective mass were also beneficial for improving quantum efficiency and reducing dark current. Recently, high quantum efficiency up to 17% was demonstrated possible for p-type QDIPs [180].

QDIPs with DWELL active region were proposed to improve the detection wavelength tunability, particularly at longer wavelengths; the typical detection wavelength at ~6 μm can be red-shifted to over 9 μm with InGaAs strain relief layers [181, 182]. Recently, DWELL photodetectors turned out to have advantages beyond wavelength tuning. For example, an overall increase of absorption volume of about two times can be achieved by adopting a low-strain active region DWELL structure [183]. Raghavan *et al* and Barve *et al* also showed that low dark current and high responsivity can be obtained from DWELL photodetectors with proper design [184, 185]. With such a structure, Kim *et al* have demonstrated a very high detectivity of $3 \times 10^{11}\,cm \cdot Hz^{1/2}W^{-1}$ at 9.3 μm and extremely low noise level at 78 K [159]. By using resonant tunnelling assisted barriers, Barve *et al* reported reduced dark current by two to four orders of magnitude compared to the control sample, an impressive conversion efficiency of 26%, and a high detectivity of $2.9 \times 10^{10}\,cm \cdot Hz^{1/2}W^{-1}$ [186, 187]. Recently, Barve *et al* also reported a high detectivity of $4 \times 10^{11}\,cm \cdot Hz^{1/2}W^{-1}$ at 77 K and $\sim 10^{8}\,cm \cdot Hz^{1/2}W^{-1}$ above 200 K [188]. Over the last ten years, DWELL infrared photodetectors have been extensively explored by Krishna's research group and some of the main achievements are presented in their recent review articles [189].

Instead of using $In_xGa_{1-x}As$ capping layers, QDIPs with other capping materials have also demonstrated interesting properties and hence improved device performance. InAs/GaAs QDIPs with $GaAs_{1-x}Sb_x$ strain reducing layers were investigated by Huang *et al* [191]. The use of $GaAs_{1-x}Sb_x$ strain reducing layers can provide a better confinement

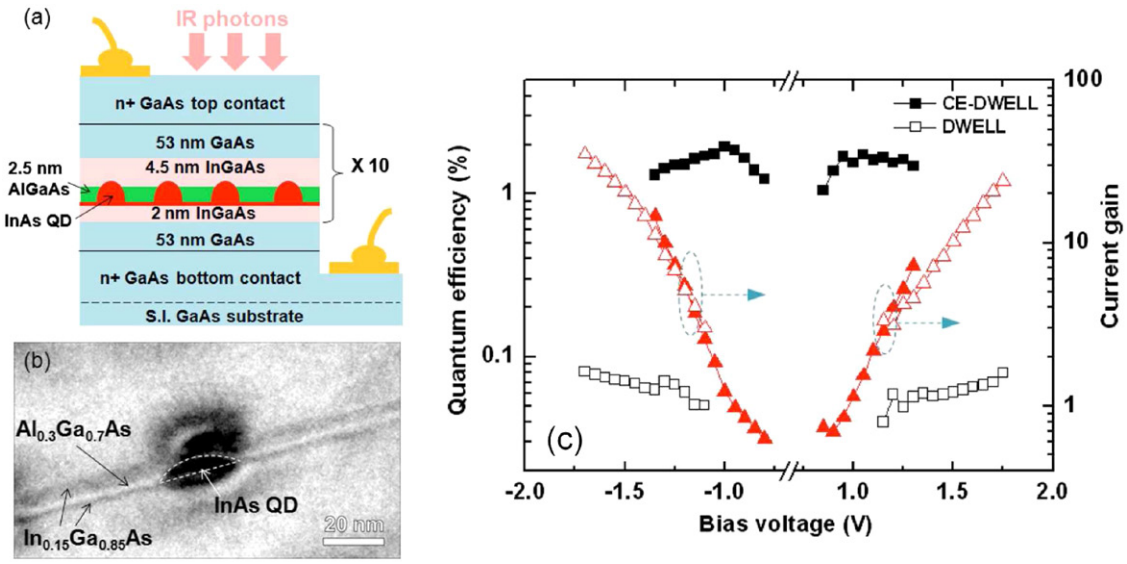

Figure 6. (a) Schematic diagram of the confinement enhanced DWELL photodetecor. (b) A TEM image of the confinement enhanced DWELL structure. (c) The current gain (triangle) and quantum efficiency (square) measured from the of the confinement enhanced DWELL (CE-DWEL) sample and reference sample (DWELL) at different voltages at 77 K. Reprinted with permission from [190]. Copyright 2008, AIP Publishing LLC.

than using $In_xGa_{1-x}As$ capping layers. The presence of the $GaAs_{1-x}Sb_x$ layer can also suppress the intermixing between In and Ga atoms and hence lead to higher QD uniformity. As a result, an enhancement of spectral responsivity to a factor of 380 was achieved. Recently, Chakrabarti *et al* explored a combined capping technique, consisting of a thick layer of GaAs and a quaternary $In_{0.21}Al_{0.21}Ga_{0.58}As$ capping layer to prevent intermixing of the QDs and the barrier material during growth. The $In_{0.21}Al_{0.21}Ga_{0.58}As$ capping layer also had a similar bandgap to GaAs, which avoids the drawback of reduced quantum confinement due to InGaAs capping. This leads to a low dark current of 1.36×10^{-6} A cm^{-2} at 77 K, the state-of-the-art responsivity of 2.16 A W^{-1}, and a high detectivity of 1.01×10^{11} cm $\cdot$ Hz$^{1/2}$ W^{-1} at 77 K were achieved [192]. The use of a confinement enhancing layer, a thin AlGaAs layer deposited in a DWELL immediately after QD formation, was also proposed and investigated with the objective of enhancing the lateral confinement of DWELLs [190]. Figure 6(a) shows the schematic diagram of the DWELL detector with 2.5 nm AlGaAs confiment enhancing layer. Figure 6(b) shows that an AlGaAs layer was formed between the QDs instead of conforming to the shape of the QDs due to the strain distribution. As a result, the confinement of the QDs in the lateral direction was improved without compromising the electron transport in the growth direction. The enhanced confinement not only enhanced the bound-to-bound transitions but also improved the escape probability. As a result, an improved quantum efficiency and a high detectivity of ~1.0×10^{10} cm $\cdot$ Hz$^{1/2}$ W^{-1}, which is about ten times higher than the reference device, were measured for the DWELL detector with confinement enhancing layers. Compared with the reference device, an improvement in quantum efficiency by a factor of 25 was also measured for the DWELL detector with confinement enhancing layers, as shown in figure 6(c) [190].

In many cases, due to the low absorption volume in QDIPs, the external quantum efficiency (QE) and the conversion efficiency (product of the photoconductive gain and QE) of the QD detectors have been low (1–5%). One of the major reasons is the defects introduced by accumulation of strain in the device, which limit the thickness of the active layer and greatly undermine the performance of QDIPs based on S–K mode [193]. Compared with S–K growth mode, droplet epitaxy is able to fabricate quantum structures from both lattice-mismatched and lattice-matched materials and quantum ring photodetectors with no built-in strain have been reported by employing droplet epitaxy [194]. The conventional low temperature droplet epitaxy growth makes it unfavourable for device applications. For example, point defects introduced by excess arsenic are commonly observed in III–V materials grown at low temperature [195]. An improved high temperature droplet epitaxy was used to improve the material quality and exciton lifetime close to 1 ns was measured [165]. With improved materials quality, quantum structures fabricated by droplet epitaxy can potentially lead to development of a new group of quantum structured photodetectors with fewer constraints in choice of materials and device design. Alternatively, nanophotonic structures are promising in providing sufficient absorption of the signal light and boosting the quantum efficiency of QDIPs. Posani *et al* developed a QDIP coupled with 2D hexagonal photonic crystals, which was used as an optical resonator to improve the device conversion efficiency [196]. The photonic crystals 'diffracts' the normally incident radiation to the in-plane direction and an increased photon absorption can be expected from the slow propagation of the in-plane radiation at the Γ point of the band structure. Localized modes in the photonic band structure could also be created by introducing 'defects' at some desired locations in the hexagonal lattice for achieving hyperspectral response. With this method, an order of magnitude increase

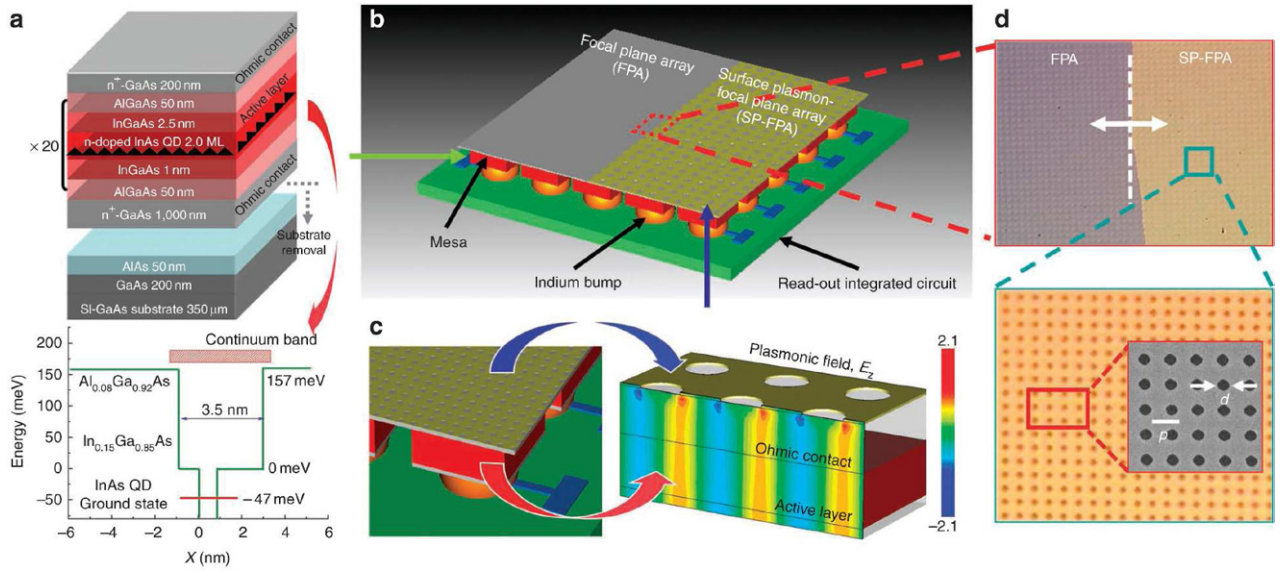

Figure 7. (a) Schematic and band diagram of a 20-layer DWELL photodetector. (b) Schematic view of DWELL FPA with half fabricated with air hole arrays flip-chip bonded on a read-out integrated circuit (ROIC). (c) Magnified illustration showing the FPA bonded to the ROIC along with the simulated surface plasmon electric field (E_z) propagating to the device active region. (d) Images of the FPA showing the non-plasmonic and plasmonic sections. The metal thickness is about 50 nm. Reprinted by permission from Macmillan Publishers Ltd: *Nat. Commun.* [202], copyright 2011.

in the photocurrent density with no change in the dark current density and a record high conversion efficiency of 95% were achieved in the QDIP coupled with photonic crystals. Surface plasmon enhanced photodetectors have also received lots of attention recently. Yu *et al* proposed a plasmonic structure made of metallic slab with opening filled with HgCdTe as the active material [197]. The slit in the metallic slab formed a Fabry–Pèrot resonator and enhanced the light absorption in the slit resonantly. In addition, the grating converted the incident electromagnetic EM waves to surface plasmons propagating towards the slit and enhanced the light absorption there. Enhancement of ~250 times in the absorption at 9.8 μm was calculated, indicating plasmonic structures can be employed to strongly enhance the performance of infrared photodetectors. Chang *et al* integrated periodic metal hole arrays with QDIPs with broadband response [198]. The response spectra of the QDIPs was distinctly modified according to the design of the plasmonic structure. However, the plasmonic effects on the device performance were not reported. Later, an experimental demonstration of thirty-fold detectivity enhancement was reported by coupling QDIPs with a thin metallic film with a periodic square array of air holes [199]. A TM-polarized evanescent field from the surface plasmon polaritons at the interface between the detector and metallic film extended into the detector active region, which significantly increased the photon absorption in the QDIPs. On the other hand, the light diffraction due to the surface plasmon effect is believed to be the dominant factor in increasing the photocurrent [200]. Nonetheless, an absolute enhancement of infrared photoresponse and detectivity >100% at the plasmonic resonance wavelength has been achieved by coupling the QDIPs with air hole arrays [201]. Subsequently, a monolithically integrated DWELL focal plane array with a metal film with air hole arrays [202]. A typical DWELL detector was grown on GaAs substrate with 50 nm AlAs etch-stop layer, as shown in figure 7(a). After the fabrication of photodetector arrays of 320 × 256, the substrate was removed by chemical mechanical polishing and then lifted off with the help of an AlAs layer. After substrate removal, half of the detector array was patterned with a 2D hole array by interferometric lithography as shown in figures 7(b) and (d). The pitch size and hole diameter were 1.79 μm and ~900 nm, respectively, which led to two resonance peaks at ~4.3 and ~6.1 μm. The simulated z-component of surface plasmon electric field was propagating to the active region, as shown in figure 7(c). The spectral response measurements show clear enhancements in the vicinity of the resonance wavelengths. A160% increase in the signal-to-noise ratio of the plasmonic FPA was demonstrated at the resonant wavelength [202]. In order to be more compatible with flip-chip bonding to the read-out integrated circuit, the authors also replaced the metallic film with air holes with a corrugated metal surface, which also led to a 15-fold enhancement of the detectivity at 77 K [203].

3.2. Multicolour quantum dot photodetectors

For many applications of infrared photodetectors, multicolour photodetectors are highly desirable for high-end infrared systems in addition to high sensitivity in specific spectral ranges. For example, two-colour photodetectors covering both near infrared and long-wavelength infrared are useful for interceptor seekers and laser designators. Some advantages of multicolour infrared detection systems include data collection in separate wavelength bands, discrimination of temperature and unique signatures of target objects [204]. Multicolour detection also enables advanced colour processing algorithms and improves sensitivity over single colour detectors [205]. Since the early 1990s, a single detector with multicolour detection

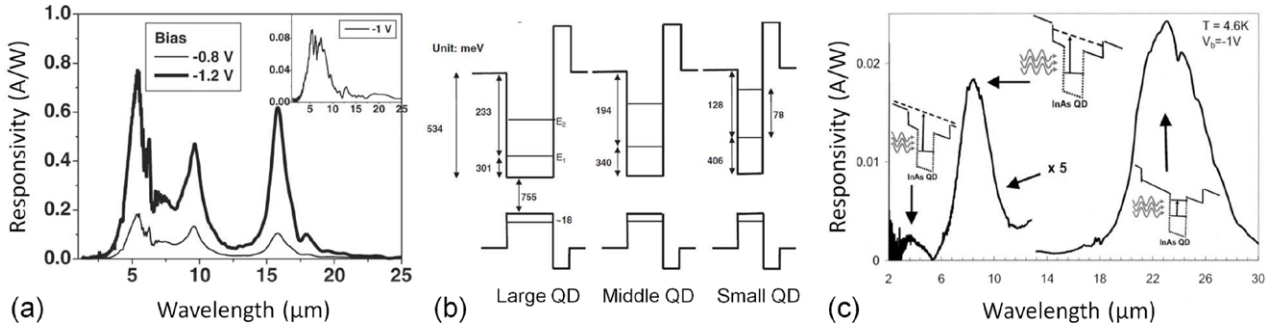

Figure 8. (a) Photoresponse of an InAs/ GaAs QDIP with 2 nm AlGaAs cap layer. The inset shows the photoresponse spectrum of a conventional InAs/GaAs QDIP without AlGaAs cap layer. (b) Schematic band diagrams of InAs/AlGaAs/GaAs QDs of different sizes (large, medium and small) fitted with PL and photoresponse peaks. (a) and (b) are reprinted with permission from [167]. Copyright 2005 The Japan Society of Applied Physics. (c) InAs/InGaAs/GaAs DWELL detector with three band photonresponse via optical transitions from different energy states as shown in the inset. Reprinted with permission from [215]. Copyright 2003, AIP Publishing LLC.

capability is of great interest and considerable progress has been made in quantum structured photodetectors. QDs can provide flexibility in tuning detection wavelength by engineering QD parameters, including QD morphology, composition, and strain. By using the unique properties of different QD materials, multicolour QDIPs have been successfully demonstrated with multiband coverage from visible to THz.

Jiang *et al* reported the first two-stack QDIP including a top stack of InGaAs/GaAs QDs and a bottom stack of InAs/GaAs QDs for multicolour detection [206]. Lin *et al* also obtained two-colour detection in two-terminal QDIPs consisted of two stacked five-periods InAs/GaAs and InAs/InGaAs/GaAs QDs similar to two-stack detectors [207]. However, multiband detection of QDIPs using a single active region would be beneficial compared to QWIPs, in which complicated designs and multiple stacks of QWs were needed for different wavelengths. Optical transitions from different intersublevels of InGaAs/InGaP QDs have been employed for multicolour detectors [208, 209]. Through optical transitions from the ground state to the quasi-bound state, a short wavelength response peaked at 5.5 μm was measured at low bias voltages. With increasing bias, a second peak around 9.2 μm was observed which can be attributed to transitions from the first excited state to the quasi-bound state. Similarly, by simply using InGaAs/GaAs QDs, multicolour photoresponse at longer wavelengths have also been reported as a result of different intersublevel transitions [210, 211]. In addition, optical absorption at different wavelengths can also be possible for QDIPs with different QD size distributions. Chen *et al* and Ye *et al* reported two band photodetection at ~5.6 and ~10 μm from intersubband transitions in the large and small QDs, respectively [212, 213]. At low bias voltages, the large QDs were preferably occupied and hence the 5.6 μm peak was dominant over the 10 μm peak. Three-band detection with narrow photoresponse peaks at 5.4, 9.5 and 15.8 μm were also reported in an InAs/AlGaAs/GaAs QDIP with three different QD size distributions [167]. As shown in figure 8(a), three narrow peaks were measured in the photoresponse spectra. PL measurements indicated existence of multimodal size distribution of the QDs, which leaded to different intersublevel transition energies as schematically plotted in figure 8(b). Unfortunately, the self-assembly nature of QDs makes it difficult to obtain precise control over the detection wavelength. An InGaAs strain-relief capping layer can be used to tailor the electronic structure of QDs in a good controlled manner [181]. With the InGaAs capping, the ground state of the QDs can be kept fixed while the position of the QW energy states with respect to the QD bound energy levels can be precisely engineered by adjusting the thickness and composition of the QW [214]. As a result, until now, DWELL photodetectors have major contribution to multicolour QDIPs. For example, Krishna *et al* reported InAs/InGaAs DWELL detector with three detection band centred at 3.8, 8.5 and 23.2 μm [215]. As shown in figure 8(c), the peaks at 3.8, 8.5 and 23.2 μm were attributed to bound-to-continuum, bound-to-quasi-bound, and bound-to-bound transitions in the DWELL, respectively [215]. By adjusting the QW width, the photoresponse peaks corresponding to bound-to-continuum and bound-to-quasi-bound can be effectively tailored [216]. The bound-to-bound was less affected by the QW width and the change in the photoresponse peak from bound-to-bound remained almost unchanged. Similar detection wavelength engineering by changing QW with can also be applied to InGaAs/GaAs/AlGaAs DWELL photodetectors [217]. DWELL photodetectors can also be designed to cover multiple infrared bands via tuning the optical transition by external voltage bias. Voltage mediated tuning of detection wavelength can be realized within a broad spectral range; photoresponse peak tuning from 8.4 to 10.3 μm and from 5.4 to 8.0 μm with small changes in the external voltage was demonstrated by using asymmetric DWELL photodetectors [218]. The progress made in multicolour DWELL photodetectors led to the successful demonstration of multicolour focal plane arrays (FPAs) [219–221].

Apart from modifying the capping layer, barrier engineering can also result in multicolour detection. A interesting approach using resonant tunnelling barriers, was successfully demonstrated with two-colour photoresponse peaks at 6 and 17 μm, more importantly, operating at room temperature [222]. In such a structure, photoexcited carriers (in the resonant-state) can be collected through a double barrier by resonant tunnelling. The resonant tunnelling barriers can effectively reduce the dark current while maintain the transport channel for photocurrent, which was critical for high temperature operation. Moreover, through adjusting the energy

levels in the resonant tunnelling barriers with regard to the resonant-state, voltage-tunable multicolour detection can be achieve. Based on this concept, voltage-tunable three-colour infrared detectors based on the so-called tunnelling-QDIP (or T-QDIP) with double barriers were demonstrated [223, 224].

Although most studies of multicolour QDIPs have been focused on MWIR and LWIR bands, photodectors sensitive to both MWIR/LWIR and visible-near infrared (vis–NIR) spectral regions are of equal importance [225–228]. It is difficult to use intersubband transitions for vis–NIR detection due to the small energy separation between the intersublevels. A dual-band photodetector with broadband response in the vis–NIR/MWIR spectral region was fabricated from InAs QDs embedded into InGaAs graded wells [229]. The MWIR band absorption was obtained from the intersubband transitions in the DWELLs while the vis–NIR band was attributed to interband transitions. By using InGaAs QDs with shallower quantum confinement, dual-band QDIPs with detection bands at vis–NIR and LWIR regions were also achieved [230].

3.3. High-operation-temperature photodetectors

Currently commercial MCT detectors and QWIPs are able to achieve multicolour detection with good detectivity. After over 15 years development, QDIPs are catching up with the performance of MCT detectors and QWIPs in terms of detectivity and multispectral detection. One of the major advantages of QDIPs over MCT detectors and QWIPs, both of which require cryogenic cooling to reduce thermal noise and obtain a reasonable signal-to-noise ratio, is the potential for high-temperature operation and high-operation-temperature QDIPs (HOT-QDIPs), which hold the promise of realizing the third-generation imaging technology. HOT-QDIPs have been demonstrated at a very early stage of its development. In 2000, only two years after demonstration of the first QDIP, Kim *et al* reported a QDIP with high detectivity at room temperature [231]. The QDIP was made of four periods of InAs QDs inserted to the 2DEG channel region of modulation-doped AlGaAs/GaAs heterostructures. The high mobility 2DEG channel significantly improved the mobility of photoexcited carriers and leaded to a high photoconductive gain [174]. Thanks to the high photoconductive gain, high detectivities of $6 \times 10^8\,\mathrm{cm \cdot Hz^{1/2} W^{-1}}$ and $5 \times 10^{10}\,\mathrm{cm \cdot Hz^{1/2} W^{-1}}$ were measured at room temperature and 80 K, respectively [231]. Although excellent HOT-QDIPs were achieved by using lateral transport in QDIPs with high mobility 2DEG channel, vertical QDIPs typically have inferior performance. Even so, by using a simple InAs/GaAs vertical QDIP structure with a single $Al_{0.3}Ga_{0.7}As$ current blocking layer, a relatively high detectivity of $\sim 10^8\,\mathrm{cm \cdot Hz^{1/2} W^{-1}}$ at 150 K was measured [172, 232]. Tang *et al* reported that by using two $Al_{0.3}Ga_{0.7}As$ dark current blocking barriers at each side of the InAs QDIP structure, near room temperature operation (~250 K) was achieved with a detectivity of $2.4 \times 10^8\,\mathrm{cm \cdot Hz^{1/2} W^{-1}}$ [233]. With two $Al_{0.2}Ga_{0.8}As$ barriers, Lu *et al* also achieved high operation temperature over 170 K of a DWELL photodetector. Due to the greatly reduced dark current, a large responsivity of $4.6\,\mathrm{A\,W^{-1}}$, high photoconductive (PC) gain over 144, and peak detectivity of $1.3 \times 10^8\,\mathrm{cm \cdot Hz^{1/2} W^{-1}}$ were measured at 170 K [234]. By increasing the number of QD layers to 70 and optimizing the material quality of the GaAs barrier, reduced dark current and increased responsivity were simultaneous attained [235]. As a result, very high detectivity of $\sim 10^{11}\,\mathrm{cm \cdot Hz^{1/2} W^{-1}}$ at 100 K and $6 \times 10^9\,\mathrm{cm \cdot Hz^{1/2} W^{-1}}$ at 200 K were measured from the device with 70 layers of QDs. A ten-layer $In_{0.6}Ga_{0.4}As$/GaAs QDIP without using any current blocking barrier also showed high operation temperatures of up to 260 K [236]. In this device, a thick GaAs spacer (60 nm) between adjacent QD layers was used. The major dark current components, including tunnelling current and thermally assisted tunnelling current, can be effectively reduced without blocking the photocurrent by using the thick GaAs spacer. The measured dark current of the $In_{0.6}Ga_{0.4}As$/GaAs QDIP was over three orders of magnitude lower than a similar QDIP with only 30 nm GaAs spacer. As a result of low dark current, a high BLIP detectivity of $1.1 \times 10^{10}\,\mathrm{cm \cdot Hz^{1/2} W^{-1}}$ at 77 K and high operation temperature up to 260 K were achieved. A low dark current in a InAs/InGaAs/InAlAs QDIP grown on InP substrate also leaded to exceptional high temperature performance. At an applied bias of −1 V, there are two peaks around 3.2 and 4.0 μm, which slightly blue-shifted with increasing temperature, as shown in figure 9(a). The photoresponse intensity of the peak around 3.2 μm was barely changed with temperature while the intensity of the longer peak around 4.0 μm

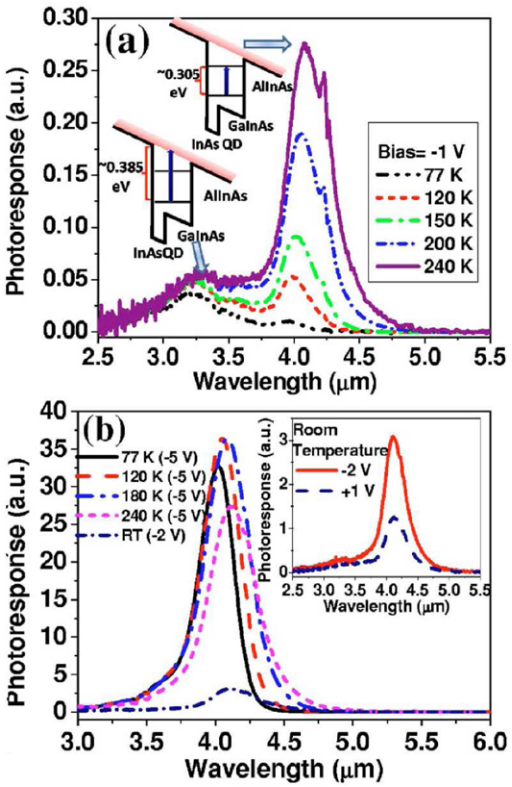

Figure 9. (a) Photoresponse spectra at different temperatures. The bias voltage is −1 V. (b) Photoresponse spectra at different temperatures for bias voltages of −5 and −2 V (room temperature). The inset shows the photoresponse spectra measured at room temperature for bias voltages of −2 and 1 V. Reprinted with permission from [237]. Copyright 2007, AIP Publishing LLC.

showed an obvious increase with temperature up to 240 K. The temperature dependence of the longer peak suggested that the corresponding optical transition was from bound-to-bound and a higher temperature helped the photoexcited electrons escape to the continuum. The low dark current in the device ensured the increase in photocurrent with temperature as high as 240 K. At even higher temperature, the significant increase in dark current due to thermonic emission caused a reduction in photoresponse as shown in figure 9(b). However, room temperature photoresponse was still achieved. A very high detectivity of $2.8 \times 10^{11}\,\mathrm{cm \cdot Hz^{1/2} W^{-1}}$ were measured at 120 K and then was reduced to $6.7 \times 10^{7}\,\mathrm{cm \cdot Hz^{1/2} W^{-1}}$ at room temperature with the peak detection wavelength around 4.1 μm [237]. The high operation temperature was attributed local trapping of dark carriers without compromising the photogenerated carriers (presumably as a result of deep confinement in QDs). Although there have been different approaches to achieve HOT-QDIPs, the general rule of thumb is to suppress dark current while maintain reasonable photocurrent at high temperature. As mentioned in previous, T-QDIPs use a resonant tunnelling barrier can filter out most dark carriers while maintain the channel of photogenerated carriers and room temperature operation at very long wavelengths in the THz spectral region has been obtained [238, 239]. However, such a method requires a good control over the resonant state with respect to the tunnelling barrier, which is challenging for self-assembled QDs. Shao *et al* recently showed that high operation temperature can be obtained by engineering the capping technique over the QDs [240]. With a proper capping material, the QD geometry and the quantum confinement can be optimized by suppressing intermixing. A quaternary InAlGaAs capping layer was found to be effective in such a role and a detectivity of $\sim 1 \times 10^{9}\,\mathrm{cm \cdot Hz^{1/2} W^{-1}}$ at 77 K and $7.2 \times 10^{7}\,\mathrm{cm \cdot Hz^{1/2} W^{-1}}$ at 250 K with peak wavelength $\lambda_p = 3.2\,\mu$m was achieved from InAs/InAlGaAs/GaAs QDIPs [240]. Likewise, by improving the quantum confinement of QDs with a thin $Al_{0.3}Ga_{0.7}As$ capping layer, high operation temperature of 240 K was achieved with peak detectivity of $1.4 \times 10^{7}\,\mathrm{cm \cdot Hz^{1/2} W^{-1}}$ at ~8 μm [241].

With the significant developments of QDIPs in the last 15 years, HOT-QDIPs with operation temperature over 200 K and up to room temperature can be obtained via a variety of approaches at different spectral regions. QDIPs with high responsivity, low dark current, and high operation temperature currently can provide all the ingredients of a third-generation detection technology.

4. Quantum dot solar cells

Although both QD lasers and QDIPs have been well explored in the 1990s, the reports on QDSCs were not available until early 2000s. The use of QDs for photovoltaic application was motivated by the idea of using sub-bandgap transitions to absorb otherwise wasted lower energy photons and improve short circuit current (J_{sc}) [242, 243]. Since 2000, QDSCs have gained increasing attention with the mature of self-assembly of QDs and better understanding of the operational principles of the devices. Till now, although much improved short circuit currents have been achieved with QDs, there are a number of fundamental issues associated with QDSCs remain unsolved. In this section, the major achievements as well as challenges for the implement QDs in solar cells for high efficient solar energy harvesting will be discussed.

4.1. Principles and advantages of quantum dot solar cells

A QDSC is very similar to the quantum well solar cell (QWSC) initially proposed by Barnham and Duggan in 1990, where multiple layers of QWs or QDs of smaller bandgap are imbedded in the intrinsic region or depletion region of a p–i–n or p–n single homojunction solar cell of larger bandgap [244]. For high-energy photons, the quantum structured solar cells behave like a conventional single junction cell. However, for light with energy smaller than the matrix bandgap, the inserted quantum structures make photon absorption in the solar cells still possible. The QWs or QDs enable additional photon absorption through an extended solar spectral coverage while the bulk p–i–n junction still acts as a normal photovoltaic cell, which can be considered equivalently as a current source and a homojunction solar cell placed in parallel. Aroutiounian *et al* developed a theoretical model of QDSCs based on self-assembled InAs/GaAs system [243]. Like QWSCs, the additional absorption from the QDs can give an increase in short circuit current J_{sc} with negligible loss in open circuit voltage (V_{oc}). Under one sun, AM 1.5 condition, the model showed a high conversation efficiency of 25% for the QDSC compared to 19.5% for the cell without QDs. However, no clear advantage of QDSCs over QWSCs is given. In addition, the carriers generated in the QDs were assumed to be collected via the build-in field, but it is still under debate whether non-optical extraction of photogenerated carriers from the QDs can have a positive contribution to the overall solar cell efficiency [245].

The major difference between QWSCs and QDSCs lies in 3D quantum confinement in QDs. The QD system with discrete density of states, at least in an ideal case, can potentially be used to form three quasi-Fermi levels as required by intermediate band solar cells (IBSCs) proposed by Luque and Martí [242, 246]. The IBSC consists of an intermediate energy band in the middle of the bandgap of ordinary semiconductor p–n junction. The additional energy band lies in the forbidden gap assists absorption of photons with energy smaller than the bandgap. As shown in figure 10(a), transitions from the valence band to conduction band can be completed by absorbing two sub-bandgap energy photons, through valence band to the intermediate band and then from the intermediate band to the conduction band. Together with conventional photon absorption directly from the valence band to conduction band, the addition photon absorption via the intermediate band more effectively utilizes the solar spectrum and improves the short circuit current of the solar cell. In an IBSC, the two-photon absorption process does not only result in a better utilization of the solar spectrum but also conserve the V_{oc}. As plotted in figure 10(b), Luque and Marti calculated a theoretical efficiency of 63%, well exceeding the Shockley–Queisser model efficiency, from an ideal IBSC [242]. The thermodynamic

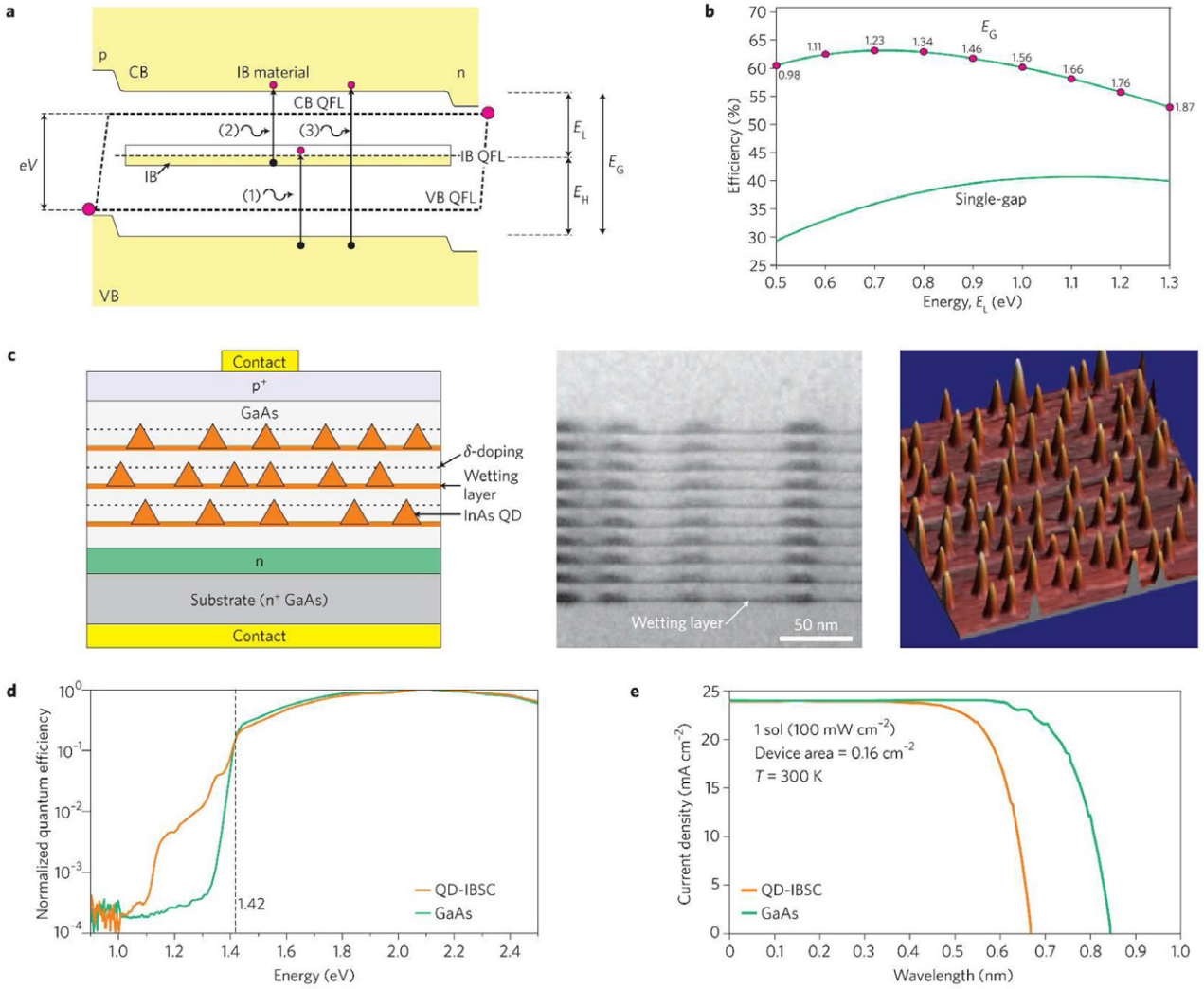

Figure 10. (a) Schematic of the band diagram of an IBSC. (b) Limiting efficiency for IBSC and single-gap cells as a function of sub-bandgap E_L. (c) Schematic of a QD IBSC along with TEM and AFM images of the QDs. (d) General quantum efficiency of a QD-IBSC and a control GaAs reference solar cell. (e) Current–voltage characteristics of a QD-IBSC and a reference solar cell. Reprinted by permission from Macmillan Publishers Ltd: Nat. Photon. [246], copyright 2012.

efficiency limit of ideal IBSCs can be extended to nearly 80% with more IBs [247]. The concept of IBSCs has inspired intensive research efforts, and QDSCs, among various techniques, have been favoured and most studied to implement the IBSC concept. The discrete confined energy levels of the QDs other than QWs can be utilized as an intermediate hand. Unlike QWSCs, the extraction of photogenerated carriers in the potential wells can take place via a second photon excitation. Another advantage of QDs over QWs is that the intersubband transitions in QWs cannot be excited by normal incident photons due to the selection rule. In addition, QDSCs may be advantageous because of improved radiation hardness and collection efficiency [248, 249]. Along with the good radiation hardness, the possible optimization of V_{oc} and J_{sc} independently in a QDSC makes it good candidate for replacing GaAs sub-cell in existing InGaP/GaAs/Ge multi-junction solar cells for space applications [250–252]. The well-established fabrication methods of QDs by epitaxy and the rich knowledge learned from QWSCs also contribute to the current popularity of QDSCs. Most of QDSCs to date have been fabricated using the In(Ga)As/GaAs QD system, which is also the most used for other optoelectronic devices. A general QDSC structure and microscopy images of QDs are shown in figure 10(c), where multiple layers of InAs/GaAs QDs with good material quality were imbedded in the middle of a GaAs p–n homojunction. Although the energy transitions deviate from the optimal values for an ideal IBSC, self-assembled QD techniques are well developed and Hu *et al* showed that InAs/GaAs QDSCs can have a peak efficiency of 52.8% given a sufficient thick InAs/GaAs QD layer and a high absorption coefficient of the intersubband transition [253]. Till now, the basic operating principles of the IBSCs have been demonstrated by the In(Ga)As/GaAs QD system. For example, Luque *et al* have experimentally demonstrated evidences for current generation from sub-bandgap photons and co-existence of three uncoupled quasi-Fermi levels in an InAs/GaAs QDSC [254]. Although the presented evidence, it has been questioned recently [255]. In 2006, Martí *et al* also demonstrated the first observation of photocurrent from two-photon absorption via confined QD energy levels at a temperature of 36 K [256]. Therefore, QDs

are one of the best candidates for developing high efficiency solar cells, e.g. IBSCs. Even so, there are three major problems associated with QDSCs [257]:

(1) short lifetime of charge carriers;
(2) weak photon absorption through the QD energy levels;
(3) thermal coupling between the QDs and bulk host materials at room temperature.

Particularly, the thermal coupling for In(Ga)As/GaAs QD-IBSCs largely undermines their potential. The typical transition energies of In(Ga)As/GaAs QDs are ~0.30, ~1.1 and 1.40 eV. The small conduction band offset of ~0.3 eV leads to a significant voltage loss due to thermal coupling of the QD states and the continuum states, as shown in figure 10(e). In addition, QDs fabricated by the conventional S–K mode have a few drawbacks for QD-IBSC applications. Self-assembled S–K QDs are not truly three-dimensionally confined quantum structures due to the presence of a thin wetting layer. As shown in figure 10(d), the intersubband absorption is rather poor due to small absorption volume and its contribution to total cell current is only around 1% or even less [41]. The strain field of the S–K QDs is not uniform which create strain gradients in the QDs and the matrix material. Such strain gradients then change the localization of carrier wave functions and further affects carriers' capture mechanisms, thermalization processes, and electron–phonon interaction in QDs [258]. Moreover, accumulated strain in S–K QD growth introduces various types of defects limiting the maximum number of QD layers can be incorporated in devices [165]. Therefore, to tackle the issues, many new approaches and designs have been taken to solve these issues in the last a few years. The major research activities have been focused on improvement of sub-bandgap photon collection and preservation of open circuit voltages V_{oc}, which will be reviewed separately in following sections.

4.2. Enhancement of short-circuit current in quantum dot solar cells

Research into QDSCs was strongly linked to the second phase of IBSC research. QDSCs have been investigated extensively as IBSC prototypes and examine the basic operating principles of the IBSCs for last ten years [259]. Despite distinct quasi-Fermi levels associated with each band in QD system, the early work has generally shown that QDs are detrimental to cell performance due to non-radiative recombination, low QD density, and non-optimized QD filling condition [260]. An attempt to increase absorption with more layers of QDs dramatically degrades the device characteristics because of progressive structural damage as strain built up [261]. Wei *et al* and Sablon *et al* investigated enhanced photon absorption from quantum dots embedded in high-energy band gap AlGaAs fence layers [262, 263]. The proposed quantum-dot-in-a-fence (DFENCE) heterostructures which consist of InAs QDs enclosed by thin $Al_xGa_{1-x}As$ 'fence' layers were predicted theoretically to enhance current generation from the QDs without the need for a large number of QDs [262]. However, the DFENCE structure did not show a clear positive impact on the short circuit current of the QDSCs, even though the thermal extraction of carriers was suppressed due to improved quantum confinement [263].

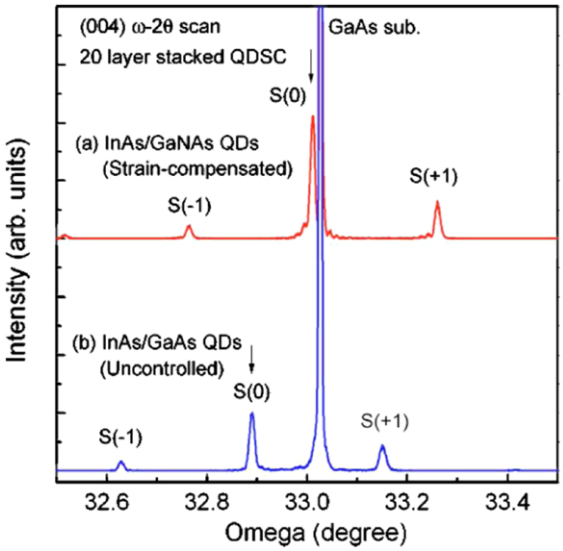

Figure 11. Symmetric (0 0 4) XRD patterns for 20 stacked layers of InAs QDs with (a) $GaN_{0.01}As_{0.99}$ strain compensation layers and (b) GaAs spacer layers, respectively. $S(x)$ indicates the xth-order satellite peak. Reprinted with permission from [264]. Copyright 2008, AIP Publishing LLC.

In order to solve this issue of low photon absorption below the host bandgap, several research groups demonstrated improved photocurrent in quantum dot solar cells with strain-compensation layers. Laghumavarapu *et al* utilized GaP strain compensation layers in a three stack InAs/GaAs QDSCs [265]. Although the device performance was still much worse than the control GaAs cell, the improved QDSC performance with strain compensation layers demonstrated the potential of this method. The GaP strain compensation layers were later used in a QDSC with 50 layers of QDs [266]. Good structural and optical properties were measured by transmission electron microscopy and photoluminescence indicating the effectiveness of the strain compensation method in improving QD quality. However, a rather poor quantum efficiency spectrum in the blue region required further optimization. Popescu *et al* also grown strain-balanced $In_{0.47}Ga_{0.53}As/GaAs_{1-x}P_x$ QDs on GaAs (3 1 1) substrate [267]. Good material quality and QD uniformity were obtained but no improvement in solar cell performance was measured due to deviation from the ideal energetic locations of IBSCs as well as the poor absorption between QD-confined electron states and host CB. A promising five stack QDSC with GaP strain compensation layers was demonstrated soon with no degradation in short circuit current [268]. Oshima *et al* also demonstrated QDSCs with more stacks of QD layers (up to 100 layers) using dilute nitride GaAsN strain compensation layers [264, 269]. As shown in figure 11, the replacement of GaAs with GaAsN of slight smaller lattice constant effectively compensated the strain introduced by QD layers of large lattie constant grown on GaAs substrates. Distinct improvement in photocurrent beyond GaAs band edge (also accompanied with QE in the short wavelength region) was achieved and the contribution of QDs to short circuit current was estimated

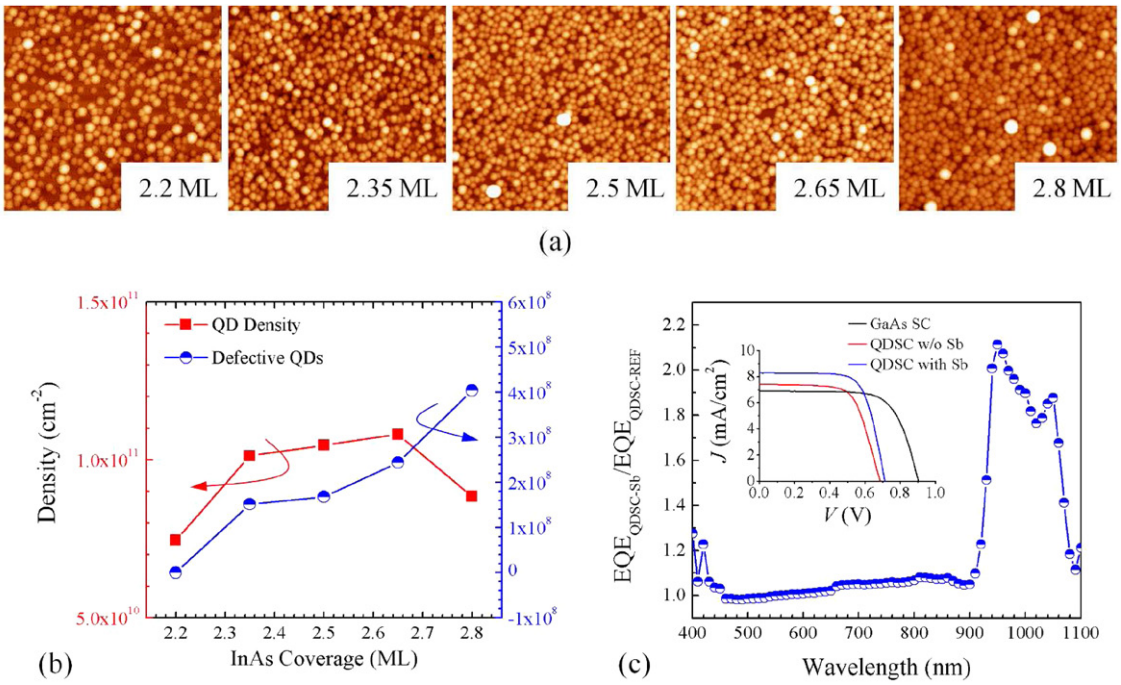

Figure 12. (a) AFM images ($1 \times 1\,\mu m^2$) of high density QDs grown with Sb pre-deposition at 485. The InAs coverage in the AFM images from left to right is 2.2 ML, 2.35 ML, 2.5 ML, 2.65 ML and 2.8 ML, respectively. (b) Coherent QD density and defective QD density as a function of InAs coverage. (c) External quantum efficiency enhancement factor of the high density QDSC compared to a control QDSC with normal QD density. The inset is current–voltage characteristics of the QDSCs and GaAs solar cells [278].

as high as 2.47 mA cm^{-2} [264]. Although the improvement in J_{sc} is highly favoured by multi-junction solar cells, it has been argued that GaAsN-contained QDSCs may not fall into the scope of realizing IBSCs due to the difficulty in recovery V_{oc} [270]. It should be worthy to mention that in the same time period, the dislocation-free vertically coupled QDs with no strain compensation layer have leaded a ~1% gain in the short-circuit current density for the first time in QDSCs [271]. Distinct improvement in short-circuit current density has also been achieved by highly stacked $In_{0.4}Ga_{0.6}As/In_{0.2}Ga_{0.8}As$ ($In_{0.4}Ga_{0.6}As$) QDs up to 50 (30) layers without using a strain balancing growth technique [272, 273]. Recently, the authors reported highly stacked $In_{0.4}Ga_{0.6}As$ QDs with no dislocations up to 400 layers and improvement in J_{sc} up to 150 layers [274]. Unfortunately, the significant degradation in open circuit voltage V_{oc} did not lead to an overall improvement in solar cell efficiency [272]. Through optimization of QDs together with strain balancing technique, strain induced defects were minimized and voltage loss was kept minimal [275]. As a result, enhanced J_{sc} and slightly reduced V_{oc} were obtained from a ten-stack InAs/GaP/GaAs strain-balanced QDSC with comparable efficiency to that of the control GaAs cell. Given that only ten layers of QDs were used, with an increase in QD layers, the optimized strain compensation technique is promising to achieve high efficiency QDSCs exceeding the GaAs homojunction solar cell. Recently, a 40-layer QDSC with reduced InAs coverage and GaP strain compensation layers exceeded the baseline GaAs cell by 0.5% absolute efficiency [276].

An alternative for increasing sub-bandgap photon absorption in QDSCs would be to increase in-plane density of QDs. Through optimization of QD growth temperature and V/III flux ratio, a high QD sheet density of 7.0×10^{10} cm^{-2} was obtained in a five stack QDSC [277]. However, due to the formation of defective QDs and low overall absorption volume in the QD region, no improvement in the J_{sc} was demonstrated. Growth of high-density QDs mediated by Sb deposition was recently demonstrated and nearly defect-free QDs can be grown with an in-plane density over 1×10^{11} cm^{-2} [278]. Figure 12(a) shows the AFM images of high density QDs grown with Sb pre-deposition. The InAs coverages were varied to achieve a high areal density of QDs and to avoid formation of defective QDs. As shown in figures 12(a) and (b), the coherent QD density can be in the order of 1.0×10^{11} cm^{-2} and the defective QD density is slightly over 1.0×10^{8} cm^{-2} with the optimized InAs coverage, e.g. 2.35 ML. Distinct improvement in J_{sc} of a 20 layer QDSC using the Sb-mediated QD growth technique has been demonstrated compared to the GaAs control device. As shown in figure 12(c), in the absorption spectral region of the QDs, the EQE of the solar cell with high density QDs was nearly doubled compared to a QDSC with normal QD density. Submonolayer (SML) QDs, normally fabricated by depositing strained In(Ga)As with surface coverage less than one monolayer in GaAs matrix, are another promising approaching to increase in-plane QD density. The SML QDs possess several advantages, including high density, high uniformity, absence of the wetting layer, and adjustable aspect ratio. Therefore, SML QDs have emerged as a promising low-dimensional nanostructure other than the conventional S–K QDs and QWs in laser and photodetector applications [279, 280]. Solar cells incorporated with multi-stacked InGaAs/GaAs SML QDs were demonstrated recently [281]. Compared with a conventional QWSC, SML QDSC has shown improved structural

quality and better efficiency due to the partial strain relaxation through formation of SML QDs. The high density SML QDs are thus promising in improving the sub-bandgap photon absorption in QDSCs. In combination with multi-stacking QD layers using strain compensation technique, these methods are expected to enhance the J_{sc} to the extent that the loss in V_{oc} can be compensated.

Engineering the QDs locally can also leaded to enhancement in short circuit current. Doping in the QD region with n-type dopants have shown a distinct increase in J_{sc}, which was explain by reduced nonradiative recombination losses and dark current or a formation of build-in field [282, 283]. In addition to an increase of collection efficiency of sub-bandgap photon and suppression of photoelectron, photocurrent gain via hot electrons was also reported very recently in a n-type doped QDSC [284]. Although further investigation may be required to fully understand the mechanism for the improvement, modification of the carrier dynamics is one of the methods should be considered in future QD-IBSC design. Replacing the type-I QDs with type-II QDs is also an object of high interest to researchers worldwide [285–288]. The absorption coefficient from extended states to bound states was over 100 times stronger in type-II QDs than type-I QDs [289]. With the parameters based on InAs/GaAs system, absorption via extended states to bound states in type-II QDs was much weaker than the absorption between bound states in type-I QDs (about ten times) [289]. However, there is no physical rule against finding a material system with stronger transitions between extended states to bound states. As a result, type-II QDSCs may be attractive for higher photocurrent generation without any reduction of V_{oc} from the valence band as in type-I QDSCs. Furthermore, long carrier lifetime up to 200 ns have been demonstrated in type-II QDs which can be additional advantages for carrier collection in type-II QDSCs [290]. Apart from the strained S–K QDs, strain-free quantum structures fabricated by droplet epitaxy have been proposed as well [291]. Photocurrent generating from the GaAs quantum structures was clearly demonstrated in quantum efficiency spectra [292–294]. Although improvement are needed in material quality as well as in-plane QD density to have a positive impact on the device performance, the two-photon absorption observed in strain-free GaAs/AlGaAs QDSCs opens new opportunities for QD based solar cells [294]. Droplet epitaxy QDs can also be grown with no wetting layer, which is also favoured for QD-IBSCs. Mainly GaAs/AlGaAs system has been studied so far but other lattice-matched materials can be explored as well.

Enhancement in short circuit current can also be accomplished by light trapping techniques. Metallic nanoparticles have been proposed to enhance absorption in QDs for realizing IBSCs. The scattered near field potential from metal nanoparticles can lead to a significant absorption enhancement factor in QDs up to ~300 times if they are placed in close vicinity [295]. The improvement in optical path can also significantly releases the burden of growing ultrahigh density of strained QDs [259]. As shown figure 13, the QD density need be improved by a factor of 1000 to achieve high efficiency QDSC exceeding the Shockley–Queisser limit, if there

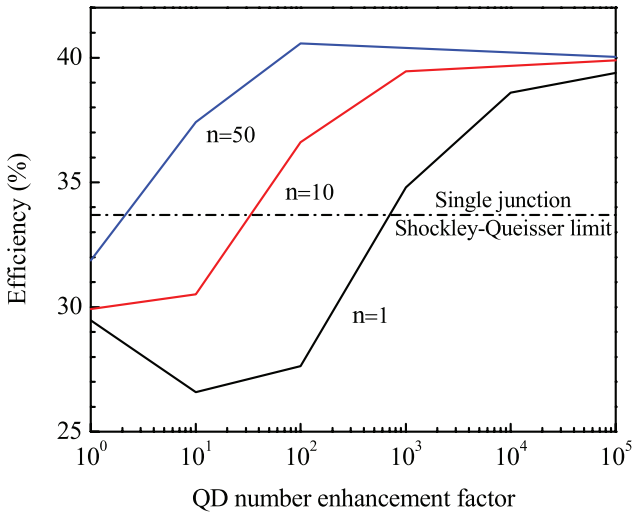

Figure 13. Efficiency of QD-IBSCs as a function of QD number enhancement factor, the factor by which the QD density is increased compared to the typical QD density of $4 \times 10^{10}\,cm^{-2}$, for different absorption enhancement factors (n) [259].

is no optical absorption enhancement. With optical absorption enhancement factor of 10, the QD density still need to be improved by a fact of about 30 to obtain a high efficiency QDSC. Given a high optical absorption enhancement factor of 50 or higher, the QD density only need to be enhanced by a few times, which can be experimentally achieved by current epitaxy growth techniques, to realize a higher efficiency than the Shockley–Queisser limit. In practical thin film QDSCs, metallic nanoparticles cannot be placed close enough to QDs to achieve such an improvement. On the other hand, metallic nanoparticles can be used as effective light scatter for light trapping [296]. Both Ag and Au nanoparticles were used to modify the surface of InAs/GaAs QDSCs by chemical linkers (figure 14(a)) [297]. Due to effective light forward scattering, an improvement in J_{sc} was achieved for both types of metallic nanoparticles. Figure 14(b) shows that spectral enhancements in quantum efficiency of QDSCs deposited with metallic nanoparticles corresponding to the resonance wavelengths of Au and Ag nanoparticles, respectively. However, the non-optimized nanophotonic architecture mainly improved the spectral region for GaAs and the improvement in long-wavelength region was marginal (figure 14(b)). A more pronounced improvement in the QD wavelength region was achieved by fabricating Ag nanoparticles over a TiO_2 layer to red-shift the plasmon resonance wavelength [298]. Using TiO_2/Ag layer as a back reflector, the improved long wavelength photon absorption in the QDSCs leaded to relative 5.3% enhancement in J_{sc}. Very interestingly, without fabrication of additional photonic structures, epitaxial lift-off QDSC thin film along with metal contacts can act as resonance cavity which was considered to be responsible for an apparent J_{sc} improvement [299]. A high efficiency was also achieved from an InAs/GaAs QDSC by using a brag reflector centred on 920 nm and shifting the QDs to the base layer. As a result, Lantratov *et al* have demonstrated a vertically coupled QDSC with a maximum efficiency of 24.93% (AM 1.5 D, 30 suns), which was slightly lower than the efficiency of the control GaAs solar cell (25.75% at

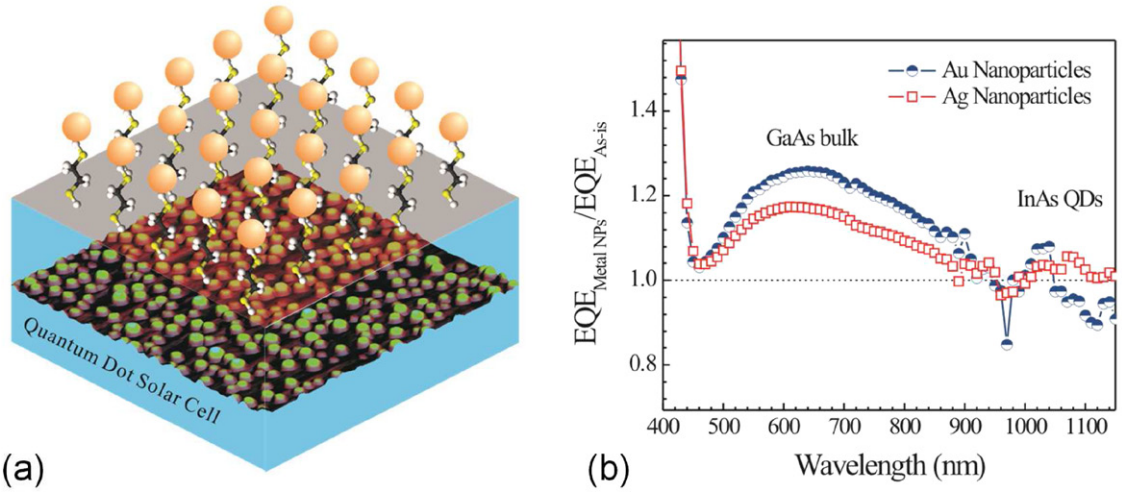

Figure 14. (a) Schematic of nanoparticles attached to a QDSC surface with chemical linkers. (b) EQE enhancement factor of the QDSCs coupled with Au and Ag nanoparticles compared with the control QDSC [297].

AM1.5 D, 10 suns). The use of the brag reflector demonstrated ~2% increase in J_{sc} due to QD absorption in the long-wavelength optical region [300]. Light trapping and concentration in the long-wavelength spectral region may lead significant improvement in the contribution of QDs through optimization the design of surface photonic structures.

4.3. Open circuit voltage recovery in quantum dot solar cells

Even though the various methods discussed previously have some merits in improving photocurrent, current QDSCs have only demonstrated marginal enhancement, if not degradation, in overall efficiency. The clear drop in open circuit voltage after adding QDs has largely undermined the photocurrent gain in the cell even for the state-of-the-art QDSCs. Although very much undesired, such a voltage loss is expected even for ideal IBSCs as the intermediate energy level plays a double role in device function [301]. While the intermediate energy band opens a path for current generation from sub-bandgap photon absorption, it also acts as a new channel for recombination. The voltage loss observed in an ideal IBSC or QDSC can be reduced at concentrated light illumination as the recombination via intermediate band(s) diminishes at high current density [41, 301]. However, the voltage loss in current literature is generally higher than expected, which is caused by additional nonradiative recombination paths in the QDSCs [302].

Apart from the radiative recombination through the intermediate band(s) in an ideal IBSC case, there are also other factors contributed to V_{oc} degradation including:

(1) non-radiative recombination due to defects;
(2) closely packed confined energy levels of holes within the valence band;
(3) continuous energy levels of the wetting layer forming below the conduction band;
(4) dominant non-optical excitation, via thermal or/and field-assisted extraction, from intermediate band to conduction band prevents quasi-Fermi level split.

The early development of QDSCs suffered quite a lot from significant voltage loss due to non-radiative recombination from strain-generated defects [266]. Over the time, the problem diminishes thanks to the significant progresses made in fabrication of high quality multi-stack QDSCs [275, 303]. Due to the confined hole states, the reduction of the effective bandgap energy is currently of less a concern because QD material systems with negligible valence band offset are already available with little difference in fabrication from the standard In(Ga)As QDs [304, 305]. Regarding to the wetting layer, an AlAs cap layer deposited over InAs QDs led to the elimination of the wetting layer formation. In a 20-stack InAs/GaAs QDSC with AlAs cap layer, an enhancement of V_{oc} to 0.79 V was obtained compared to 0.69 V for a QDSC without AlAs cap layer [306]. From quantum efficiency spectrum, the wetting layer absorption nearly completely disappeared upon using AlAs cap layer. The enhanced V_{oc} and disappeared absorption at wetting layer wavelength region could represent an important step towards the implementation of QD-IBSCs, despite a slight reduction in J_{sc} due to reduced photocurrent contribution from wetting layer and non-optimized growth conditions for AlAs cap layer.

The major issue for the voltage loss facing QDSCs is the non-optical link between the confined states in QDs and the continuum states. The weak optical pumping rate from the intermediate state(s) to the continuum is overwhelmed by the much stronger non-optical generation rate via thermal and/or field-assisted extraction. It has been shown that very strong photocurrent were presented at room temperature, and by comparing with the low temperature photoresponse measurement, the strong photon current generated from QDs at room temperature was caused mainly by thermal-assisted interband transitions from valence band to confined QD/or wetting layer electronic states [307]. Okada *et al* estimated a high ratio of 1 : 20 between the optical and non-optical transitions at room temperature [282]. A very interesting observation in the investigation carried out by Okada *et al* was the observation of photocurrent generation from two-photon absorption process under AM 1.5 one sun illumination in a Si-doped QDSC but

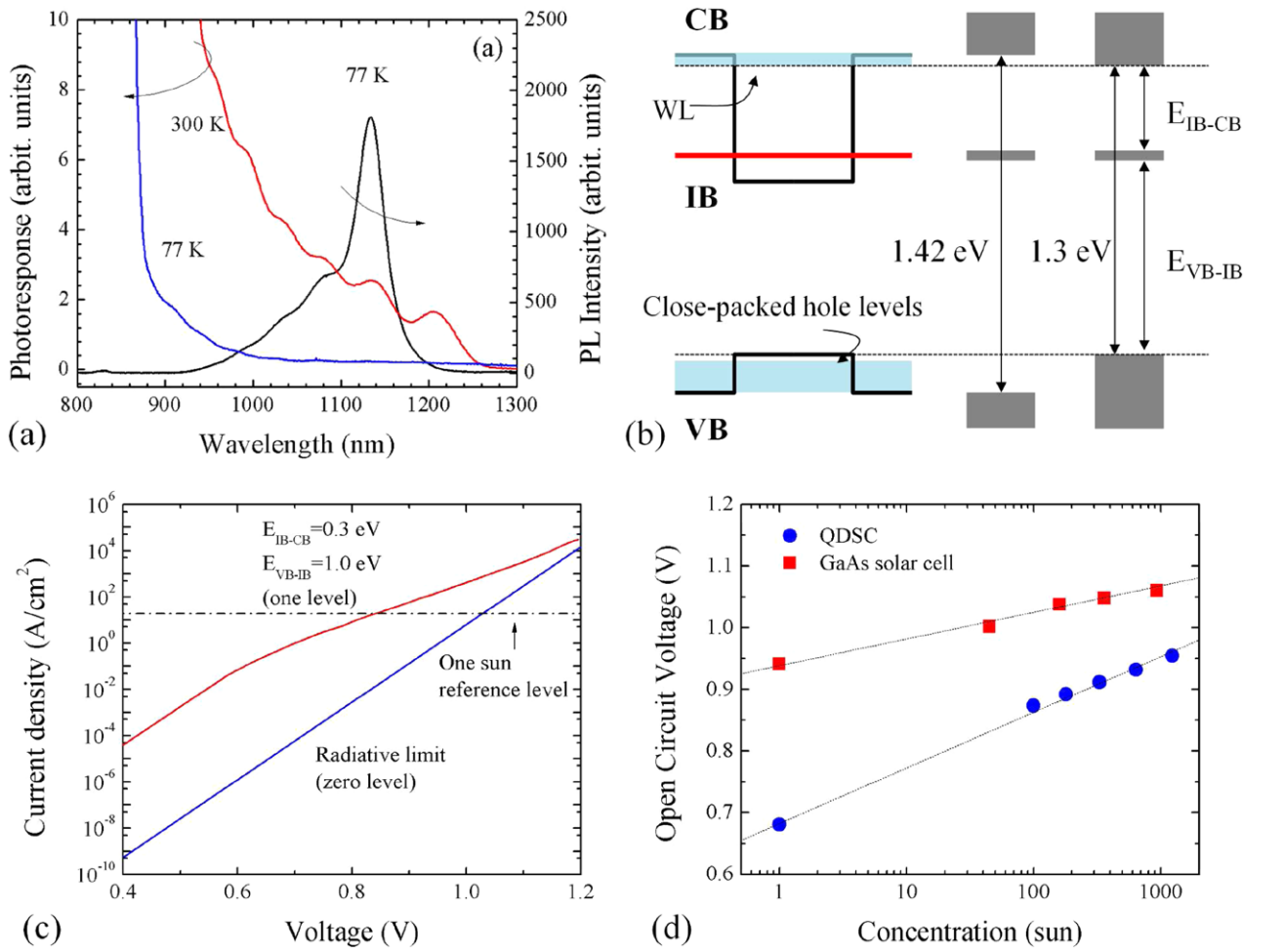

Figure 15. (a) PL spectrum measured at 77 K plotted along with the photoresponse spectra measured at 300 and 77 K of a QDSC. Adopted with permission from [307]. Copyright 2012, AIP Publishing LLC. (b) Illustration of transition energies in a typical QDSC. (c) The current–voltage characteristic of an IBSC with one intermediate level and a single junction control cell [301]. (d) Measured V_{oc} as a function of concentration [312].

not in a undoped QDSC of same structure [282]. The observation of two-photon absorption processes in the doped QDSC at room temperature was thus attributed to the partial filling of the QDs. Although no current–voltage characteristics under illumination was reported, the dark current results indicated an improved open circuit voltage would be expected due to reduced nonradiative recombination losses and dark current in the doped QDSC. A recent study of Si-doped QDSCs by Yang *et al* has clearly shown both improvement of J_{sc} and V_{oc} with appropriate doping level [308]. The improvement in V_{oc} was also attributed to reduced nonradiative recombination because Si dopants was claimed to fill the trap states and partially relax the strain. Beyond the optimized doping levels, nonradiative recombination could be created and a reduction in J_{sc} was measured but with V_{oc} unchanged. Recently, we have also shown that V_{oc} can be nearly recovered with similar doping level as the work by Yang *et al* [309]. However, the nonradiative recombination was found to be increased by adding dopants, which contradicts with the previous studies [282, 308]. The discrepancy may arise from the difference in doping conditions during material growth. Nevertheless, the improvement in V_{oc} together with more nonradiative recombination leads us to speculate that the improvement in V_{oc} was caused by a change of carrier dynamics in the QDs. By measuring temperature-dependent time PL, an improvement in activation energy with increasing doping was observed, which indicated that a potential barrier forming around the QDs as a result of external doping. Transient PL measurements at l0 K and room temperature have also shown the capture of photon-excited carriers into the QD as well as the thermal activation of carriers from the QDs back into the wetting layer and/or continuum were restricted by intentional doping. This observation was in agreement with an early study on the doping induced change of electronic parameters of QD structures [310]. Although doping in the QD region may cause other changes of the cell that can affect the device characteristics, e.g. depletion region width, engineering of carrier dynamics of QDs locally can potentially lead to reduced thermal coupling for operation of QD-IBSC at room temperature. Besides the effect of doping, the position of QDs in the p–i–n junction was shown to affect the device performance as well and thus need to be considered in design of high efficient QDSCs [311].

It has also been shown that voltage recovery occurs with increasing concentration for a QD-IBSC [301]. However,

experimentally, the full voltage recovery relative to a control cell was only achieved at 77 K and lower [313, 314]. The absence of quasi-Fermi level splitting in the InAs/GaAs QDSC was the equivalent of reducing the cell bandgap and a sign of quasi-Fermi level splitting and partial voltage recovery under concentrated light irradiation begun to appear at a temperature as low as 150 K [315]. Other material systems, such as InAs/AlGaAs, may be considered to solve the loss in open circuit voltage. AlGaAs can be adjusted to match the optimum host bandgap of IBSCs and the enlarged conduction band offset between InAs and AlGaAs is beneficial for suppressing thermal escaping of carrier. An increase of 140 meV in activation energy was reported from an InAs/$Al_{0.25}Ga_{0.75}As$ QDSC compared with a conventional InAs/GaAs QDSC [315]. The improved confinement also leaded to the observation of two-photon sub-bandgap photocurrent up to 220 K as opposed to 140 K for the reference device. However, even when using a higher bandgap $Al_{0.25}Ga_{0.75}As$ matrix, thermal carrier escape cannot be suppressed unless the cell temperature was around 220 K or below. There are normally more than one electronic energy states in the self-assembled QDs [307, 316], and, undoubtedly, additional states facilitate the thermalization of photo-generated carriers out from QDs. As shown in figure 15(a), there are multiple peaks measured in both PL (77 K) and photoresponse (300 K) spectra. These additional peaks were attributed to optical transitions from multiple confined energy states in the QDs. When the QDSC was cooled to 77 K, the addition photoresponse peaks disappeared because of suppressed thermalization of photo-generated carriers from the multiple electronic levels in the QDs into the continuum different. It has also been shown that non-optical excitation remains the dominant carrier escape mechanisms even under photon flux far beyond the range of practical solar concentrations [317]. The significant thermal escape of carriers necessitates reducing the QD dimensions, preferably below 10 nm, so that only one electronic energy level forms in the QDs (figure 15(b)) and photo-generated carriers in the QDs from the valence band can be optically excited to conduction band instead of thermal escape at room temperature [318]. Reducing carrier relaxation rate while maintaining carrier collection efficiency also plays a critical role in achieve high efficiency QDSCs [317]. Even so, the current experimental results of the concentration measurements made with 'non-ideal' InAs QDSCs have demonstrated good promise of using them in concentrator photovoltaic modules. According to the simplified QD bandstructure shown in figure 15(b), the effective bandgap is smaller than the host semiconductor due to the presence of wetting layer and closely packed hole states. Therefore, based on this structure with only one confined electron level, at one sun illumination condition, the open circuit voltage is much smaller compared with a single junction cell made of the host semiconductor, as shown in figure 15(c). According to the detailed balance calculation by Martí *et al*, recombination via intermediate band(s) largely reduces and recombination between the conduction band to the valence band becomes dominant at high current density level [301]. Figure 15(c) shows that the open circuit voltage can be significantly recovered and approaching the limit of the single junction cell under high concentration. Experimental results also confirmed the faster recovery of V_{oc} under concentration. Figure 15(d) shows that a rapid recovery of V_{oc} of InAs/GaNAs QDSCs under concentration [312, 319]. The fast recovery of V_{oc} under solar concentration was observed in GaSb/GaAs quantum ring solar cells [320] and InAs/GaAs QDSCs [321, 322]. Moreover, high quality QDSCs with excellent diode ideality factors as low as 1.16 was measured from illumination dependent V_{oc} measurement up to 500 suns [323]. These demonstrations further support the promise of QDSCs in high efficient photovoltaic cells despite their non-ideal energy levels.

Most of the current studies have been focused on In(Ga)As/(Al)GaAs material system, which have been served as a good platform for testing the main principles of prototype QD-IBSCs. Other materials systems may also be worthy of investigation to well outperform the performance of the state-of-the-art GaAs single junction solar cells [324, 325].

5. Conclusions

In the present paper, we have reviewed the current progress in III–V QD based optoelectronic devices, including lasers, photodetectors, and solar cells. QDs are of great interest due to their atom-like electronic structure and flexibility in engineering new optical properties for high-performance optoelectronic devices. QDs can be applied to a large variety of optoelectronic devices and QD based devices can realize new functions and/or the state-of-the-art performance, that cannot be achieved, at least easily, in conventional devices based on QWs or bulk materials.

QD lasers, particularly 1.3 μm wavelength lasers, grown on GaAs substrates have made great breakthroughs in the last 15 years, which have already brought QD lasers to commercial markets. The increasingly urgent market demand for developing cost effective and reliable light sources on Si substrates has opened new challenges for QD lasers. Current advances in III–V QD lasers monolithically grown on Si demonstrate great potential for practical applications and their future in silicon photonics appears extremely bright. Future investigation of III–V QD lasers on Si substrates requires further improvement in material quality and keeping the dislocation density to a minimum, so that the device performance and reliability can meet the industrial standards.

The intense research efforts in QDs also make high-performance QDIPs possible. The fundamental advantages of QDIPs allow them to operate at higher temperatures and lower dark current than QWIPs. QDIPs are now demonstrating high performance comparable to QWIPs. In particular, the operation temperature of QDIPs has substantially outperformed QWIPs. Various issues still remain, such as insufficient quantum efficiency, and the design and fabrication of QDIPs need to be improved to fulfil their promise in third-generation infrared sensing. The coming years may witness QDIPs with performance competing on all metrics with current state-of-the-art technologies such as QWIPs and HgCdTe photodetectors.

QDSCs are the least developed compared with other types of QD optoelectronic devices, due to a number of fundamental

limitations, including the weak absorption of QDs and the severe thermal connection between the intermediate band and conduction band. Yet, there is significant progress being made in QDSCs and intermediate band based operation has been demonstrated. Further improvements in device physics, design, growth and characterization of QDSCs will be required to achieve high conversion efficiency exceeding the record value of GaAs single junction solar cells.

Acknowledgment

The authors acknowledge financial support from UK EPSRC under Grant No. EP/J012904/1 and Grant No EP/K029118/1. H Liu would like to thank The Royal Society for funding his University Research Fellowship.

References

[1] Dingle R and Henry C H 1976 *Patent Number* US3982207 A
[2] Asada M, Miyamoto Y and Suematsu Y 1986 *IEEE J. Quantum Electron.* **22** 1915–21
[3] Arakawa Y and Sakaki H 1982 *Appl. Phys. Lett.* **40** 939–41
[4] Eaglesham D J and Cerullo M 1990 *Phys. Rev. Lett.* **64** 1943–6
[5] Koguchi N, Takahashi S and Chikyow T 1991 *J. Cryst. Growth.* **111** 688–92
[6] Leonard D, Krishnamurthy M, Reaves C M, Denbaars S P and Petroff P M 1993 *Appl. Phys. Lett.* **63** 3203–5
[7] Kirstaedter N *et al* 1994 *Electron. Lett.* **30** 1416–17
[8] Matthews J and Blakeslee A 1974 *J. Cryst. Growth* **27** 118–25
[9] Ruvimov S, Werner P, Scheerschmidt K, Gösele U, Heydenreich J, Richter U, Ledentsov N, Grundmann M, Bimberg D and Ustinov V 1995 *Phys. Rev.* B **51** 14766
[10] Teichert C 2002 *Phys. Rep.* **365** 335–432
[11] Moison J, Houzay F, Barthe F, Leprince L, Andre E and Vatel O 1994 *Appl. Phys. Lett.* **64** 196–8
[12] Mirin R, Ibbetson J, Nishi K, Gossard A and Bowers J 1995 *Appl. Phys. Lett.* **67** 3795–7
[13] Ustinov V, Maleev N, Zhukov A, Kovsh A, Egorov A Y, Lunev A, Volovik B, Krestnikov I, Musikhin Y G and Bert N 1999 *Appl. Phys. Lett.* **74** 2815–17
[14] Ponchet A, Le Corre A, L'haridon H, Lambert B and Salaün S 1995 *Appl. Phys. Lett.* **67** 1850–2
[15] Sopanen M, Xin H and Tu C 2000 *Appl. Phys. Lett.* **76** 994–6
[16] Heinrichsdorff F, Krost A, Grundmann M, Bimberg D, Kosogov A and Werner P 1996 *Appl. Phys. Lett.* **68** 3284–6
[17] Heinrichsdorff F, Mao M, Kirstaedter N, Krost A, Bimberg D, Kosogov A and Werner P 1997 *Appl. Phys. Lett.* **71** 22–4
[18] Carlsson N, Junno T, Montelius L, Pistol M, Samuelson L and Seifert W 1998 *J. Cryst. Growth* **191** 347–56
[19] Marchand H, Desjardins P, Guillon S, Paultre J, Bougrioua Z, Yip R and Masut R 1997 *Appl. Phys. Lett.* **71** 527–9
[20] Kumah D P, Shusterman S, Paltiel Y, Yacoby Y and Clarke R 2009 *Nat. Nanotechnol.* **4** 835–8
[21] Jo M, Mano T, Sakuma Y and Sakoda K 2012 *Appl. Phys. Lett.* **100** 212113
[22] Somaschini C, Bietti S, Koguchi N and Sanguinetti S 2009 *Nano Lett.* **9** 3419–24
[23] Wu J, Hirono Y, Li X, Wang Z M, Lee J, Benamara M, Luo S, Mazur Y I, Kim E S and Salamo G J 2014 *Adv. Funct. Mater.* **24** 530–35
[24] Wang Z M, Liang B L, Sablon K A and Salamo G J 2007 *Appl. Phys. Lett.* **90** 113120
[25] Li X, Wu J, Wang Z M, Liang B, Lee J, Kim E and Salamo G J 2014 *Nanoscale* **6** 2675–81
[26] Lee J, Wang Z, Hirono Y, Kim E, Koo S, Dorogan V G, Mazur Y I, Song S, Park G and Salamo G J 2011 *J. Phys. D: Appl. Phys.* **44** 025102
[27] Somaschini C, Bietti S, Trampert A, Jahn U, Hauswald C, Riechert H, Sanguinetti S and Geelhaar L 2013 *Nano Lett.* **13** 3607–13
[28] Liang B L, Wang Z M, Lee J H, Sablon K, Mazur Y I and Salamo G J 2006 *Appl. Phys. Lett.* **89** 043113
[29] Heyn C, Stemmann A, Köppen T, Strelow C, Kipp T, Grave M, Mendach S and Hansen W 2009 *Appl. Phys. Lett.* **94** 183113
[30] Berryman K, Lyon S and Segev M 1997 *Appl. Phys. Lett.* **70** 1861–3
[31] Pan D, Towe E and Kennerly S 1998 *Appl. Phys. Lett.* **73** 1937
[32] Martí A, Cuadra L and Luque A 2000 *Photovoltaic Specialists Conf., 2000. Conf. Record of the 28th IEEE* (*Anchorage, AK, 15–22 September 2000*) vol 2009 pp 940–3
[33] Borri P, Langbein W, Hvam J M, Heinrichsdorff F, Mao M and Bimberg D 2000 *IEEE Photon. Technol. Lett.* **12** 594–6
[34] Zhang Z, Wang Z, Xu B, Jin P, Sun Z and Liu F 2004 *IEEE Photon. Technol. Lett.* **16** 27–9
[35] Chen S, Zhou K, Zhang Z, Orchard J R, Childs D T, Hugues M, Wada O and Hogg R A 2013 *IEEE J. Sel. Top. Quantum Electron.* **19** 1900209
[36] Chen S, Zhou K, Zhang Z, Childs D, Hugues M, Ramsay A and Hogg R 2012 *Appl. Phys. Lett.* **100** 041118
[37] Barve A V, Lee S J, Noh S K and Krishna S 2010 *Laser Photon. Rev.* **4** 738–50
[38] Ledentsov N 2011 *Semicond. Sci. Technol.* **26** 014001
[39] Akiyama T, Sugawara M and Arakawa Y 2007 *Proc. IEEE* **95** 1757–66
[40] Zhang Z, Hogg R, Lv X and Wang Z 2010 *Adv. Opt. Photon.* **2** 201–28
[41] Luque A and Marti A 2010 *Adv. Mater.* **22** 160–74
[42] Kroemer H 1963 *Proc. IEEE* **51** 1782–3
[43] Alferov Z I and Kazarinov R 1963 Application Number 950840 *Patent Number* 181737
[44] Ledentsov N, Ustinov V, Shchukin V, Kop'ev P, Alferov Z I and Bimberg D 1998 *Semiconductors* **32** 343–65
[45] Ghosh S, Pradhan S and Bhattacharya P 2002 *Appl. Phys. Lett.* **81** 3055–7
[46] Maximov M, Ledentsov N, Ustinov V, Alferov Z I and Bimberg D 2000 *J. Electron. Mater.* **29** 476–86
[47] Newell T, Bossert D, Stintz A, Fuchs B, Malloy K and Lester L 1999 *IEEE Photon. Technol. Lett.* **11** 1527–9
[48] Reithmaier J P and Forchel A 2003 *C. R. Phys.* **4** 611–19
[49] Smowton P, Pearce E, Schneider H, Chow W and Hopkinson M 2002 *Appl. Phys. Lett.* **81** 3251–3
[50] Asryan L and Suris R 1997 *IEEE J. Sel. Top. Quantum Electron.* **3** 148–57
[51] Ledentsov N 1999 *Semiconductors* **33** 946–50
[52] Ribbat C, Sellin R, Grundmann M, Bimberg D, Sobolev N and Carmo M 2001 *Electron. Lett.* **37** 174–5
[53] Beanland R, Sanchez A, Childs D, Groom K, Liu H, Mowbray D and Hopkinson M 2008 *J. Appl. Phys.* **103** 014913
[54] Maximov M V and Ledentsov N N 2004 *Dekker Encyclopedia of Nanoscience and Nanotechnology* chapter 247 (London: CRC Press) pp 3109–26
[55] Li S, Gong Q, Cao C, Wang X, Yan J, Wang Y and Wang H 2013 *Infrared Phys. Technol.* **60** 216–24
[56] Hirayama H, Matsunaga K, Asada M and Suematsu Y 1994 *Electron. Lett.* **30** 142–3
[57] Ledentsov N, Shchukin V, Grundmann M E, Kirstaedter N, Böhrer J, Schmidt O, Bimberg D, Ustinov V, Egorov A Y and Zhukov A 1996 *Phys. Rev.* B **54** 8743
[58] Huffaker D, Park G, Zou Z, Shchekin O and Deppe D 1998 *Appl. Phys. Lett.* **73** 2564–6

[59] Liu G, Stintz A, Li H, Malloy K and Lester L 1999 *Electron. Lett.* **35** 1163–5
[60] Park G, Shchekin O B, Csutak S, Huffaker D L and Deppe D G 1999 *Appl. Phys. Lett.* **75** 3267–9
[61] Mukai K, Nakata Y, Otsubo K, Sugawara M, Yokoyama N and Ishikawa H 1999 *IEEE Photon. Technol. Let.* **11** 1205–7
[62] Huang X, Stintz A, Hains C, Liu G, Cheng J and Malloy K 2000 *IEEE Photon. Technol. Lett.* **12** 227–9
[63] Huang X, Stintz A, Hains C, Liu G, Cheng J and Malloy K 2000 *Electron. Lett.* **36** 41–2
[64] Park G, Shchekin O B, Huffaker D L and Deppe D G 2000 *IEEE Photon. Technol. Lett.* **12** 230–2
[65] Liu H, Hopkinson M, Harrison C, Steer M, Frith R, Sellers I, Mowbray D and Skolnick M 2003 *J. Appl. Phys.* **93** 2931–6
[66] Liu H, Sellers I, Badcock T, Mowbray D, Skolnick M, Groom K, Gutierrez M, Hopkinson M, Ng J and David J 2004 *Appl. Phys. Lett.* **85** 704–6
[67] Liu H, Sellers I, Gutierrez M, Groom K, Soong W, Hopkinson M, David J, Beanland R, Badcock T and Mowbray D 2004 *J. Appl. Phys.* **96** 1988–92
[68] Walker C, Sandall I, Smowton P, Sellers I, Mowbray D, Liu H and Hopkinson M 2005 *IEEE Photon. Technol. Lett.* **17** 2011–13
[69] Sellers I, Liu H, Groom K, Childs D, Robbins D, Badcock T, Hopkinson M, Mowbray D and Skolnick M 2004 *Electron. Lett.* **40** 1412–13
[70] Liu H, Childs D, Badcock T, Groom K, Sellers I, Hopkinson M, Hogg R, Robbins D, Mowbray D and Skolnick M 2005 *IEEE Photon. Technol. Lett.* **17** 1139–41
[71] Freisem S, Ozgur G, Shavritranuruk K, Chen H and Deppe D 2008 *Electron. Lett.* **44** 679–81
[72] Deppe D, Shavritranuruk K, Ozgur G, Chen H and Freisem S 2009 *Electron. Lett.* **45** 54–6
[73] Park G, Shchekin O, Huffaker D and Deppe D 2000 *Electron. Lett.* **36** 1283–4
[74] Sandall I, Smowton P, Walker C, Liu H, Hopkinson M and Mowbray D 2006 *IEEE Photon. Technol. Lett.* **18** 965–7
[75] Mukai K, Nakata Y, Otsubo K, Sugawara M, Yokoyama N and Ishikawa H 2000 *Appl. Phys. Lett.* **76** 3349–51
[76] Chen H, Zou Z, Shchekin O and Deppe D 2000 *Electron. Lett.* **36** 1703–4
[77] Liu G, Stintz A, Li H, Newell T, Gray A, Varangis P, Malloy K and Lester L 2000 *IEEE J. Quantum Electron.* **36** 1272–9
[78] Shchekin O and Deppe D 2002 *Appl. Phys. Lett.* **80** 3277–9
[79] Sandall I, Smowton P, Walker C, Badcock T, Mowbray D, Liu H and Hopkinson M 2006 *Appl. Phys. Lett.* **88** 111113
[80] Smowton P M, Sandall I C, Liu H and Hopkinson M 2007 *J. Appl. Phys.* **101** 013107
[81] Sandall I, Walker C, Smowton P, Mowbray D, Liu H and Hopkinson M 2006 *IEEE Proc.-Optoelectron.* **153** 316–20
[82] Shchekin O, Ahn J and Deppe D 2002 *Electron. Lett.* **38** 712–13
[83] Shchekin O and Deppe D 2002 *IEEE Photon. Technol. Lett.* **14** 1231–3
[84] Badcock T, Liu H, Groom K, Jin C, Gutierrez M, Hopkinson M, Mowbray D and Skolnick M 2006 *Electron. Lett.* **42** 922–3
[85] Badcock T, Royce R, Mowbray D, Skolnick M, Liu H, Hopkinson M, Groom K and Jiang Q 2007 *Appl. Phys. Lett.* **90** 111102
[86] Jin C, Badcock T J, Liu H, Groom K M, Royce R J, Mowbray D J and Hopkinson M 2006 *IEEE J. Quantum Electron.* **42** 1259–65
[87] Sandall I C, Smowton P M, Thomson J D, Baddock T, Mowbray D, Liu H and Hopkinson M 2006 *Appl. Phys. Lett.* **89** 151118
[88] Smowton P M, Sandall I C, Mowbray D J, Liu H Y and Hopkinson M 2007 *IEEE J. Sel. Top. Quantum Electron.* **13** 1261–6
[89] Fathpour S, Mi Z, Bhattacharya P, Kovsh A, Mikhrin S, Krestnikov I, Kozhukhov A and Ledentsov N 2004 *Appl. Phys. Lett.* **85** 5164–6
[90] Mi Z, Bhattacharya P and Fathpour S 2005 *Appl. Phys. Lett.* **86** 153109
[91] Liu H, Liew S, Badcock T, Mowbray D, Skolnick M, Ray S, Choi T, Groom K, Stevens B and Hasbullah F 2006 *Appl. Phys. Lett.* **89** 073113
[92] Sugawara M and Usami M 2009 *Nat. Photon.* **3** 30–1
[93] Tanaka Y, Ishida M, Takada K, Yamamoto T, Song H, Nakata Y, Yamaguchi M, Nishi K, Sugawara M and Arakawa Y 2010 *Conf. on Lasers and Electro-Optics CTuZ1*
[94] Kageyama T, Nishi K, Yamaguchi M, Mochida R, Maeda Y, Takemasa K, Tanaka Y, Yamamoto T, Sugawara M and Arakawa Y 2011 *European Conf. on Lasers and Electro-Optics* PDA_1
[95] Zhukov A, Maksimov M and Kovsh A 2012 *Semiconductors* **46** 1225–50
[96] Miller D A 2009 *Proc. IEEE* **97** 1166–85
[97] Michel J, Liu J and Kimerling L C 2010 *Nat. Photon.* **4** 527–34
[98] Reed G T, Mashanovich G, Gardes F and Thomson D 2010 *Nat. Photon.* **4** 518–26
[99] Jalali B and Fathpour S 2006 *J. Lightwave Technol.* **24** 4600–15
[100] Rong H, Jones R, Liu A, Cohen O, Hak D, Fang A and Paniccia M 2005 *Nature* **433** 725–8
[101] Chen X, Li C and Tsang H K 2011 *NPG Asia Mater.* **3** 34–40
[102] Yuan Z, Anopchenko A, Daldosso N, Guider R, Navarro-Urrios D, Pitanti A, Spano R and Pavesi L 2009 *Proc. IEEE* **97** 1250–68
[103] Camacho-Aguilera R E, Cai Y, Patel N, Bessette J T, Romagnoli M, Kimerling L C and Michel J 2012 *Opt. Express* **20** 11316–20
[104] Tanaka S, Jeong S, Sekiguchi S, Kurahashi T, Tanaka Y and Morito K 2012 *Opt. Express* **20** 28057–69
[105] Chang H, Fang A W, Sysak M N, Park H, Jones R, Cohen O, Raday O, Paniccia M J and Bowers J E 2007 *Opt. Express* **15** 11466–71
[106] Tanabe K, Guimard D, Bordel D, Iwamoto S and Arakawa Y 2010 *Opt. Express* **18** 10604–8
[107] Tanabe K, Watanabe K and Arakawa Y 2012 *Sci. Rep.* **2** 349
[108] Liang D and Bowers J E 2010 *Nat. Photon.* **4** 511–17
[109] Wang W 1984 *Appl. Phys. Lett.* **44** 1149–51
[110] Fletcher R M, Wagner D K and Ballantyne J M 1984 *Appl. Phys. Lett.* **44** 967–9
[111] Deppe D, Holonyak N Jr, Nam D, Hsieh K, Jackson G, Matyi R, Shichijo H, Epler J and Chung H 1987 *Appl. Phys. Lett.* **51** 637–9
[112] Deppe D, Nam D, Holonyak N Jr, Hsieh K, Matyi R, Shichijo H, Epler J and Chung H 1987 *Appl. Phys. Lett.* **51** 1271–3
[113] Kaliski R, Holonyak N Jr, Hsieh K, Nam D, Lee J, Shichijo H, Burnham R, Epler J and Chung H 1987 *Appl. Phys. Lett.* **50** 836–8
[114] Hall D, Deppe D, Holonyak N Jr, Matyi R, Shichijo H and Epler J 1988 *J. Appl. Phys.* **64** 2854–60
[115] Sugo M, Mori H, Sakai Y and Itoh Y 1992 *Appl. Phys. Lett.* **60** 472–3
[116] Hasegawa Y, Egawa T, Jimbo T and Umeno M 1996 *Appl. Surf. Sci.* **100** 482–6
[117] Hasegawa Y, Egawa T, Jimbo T and Umeno M 1996 *Appl. Phys. Lett.* **68** 523–5
[118] Gérard J, Cabrol O and Sermage B 1996 *Appl. Phys. Lett.* **68** 3123–5
[119] Lacombe D, Ponchet A, Gerard J and Cabrol O 1997 *Appl. Phys. Lett.* **70** 2398–400

[120] Egawa T, Ogawa A, Jimbo T and Umeno M 1998 *Japan. J. Appl. Phys.* **37** 1552–5
[121] Wu J and Wang Z M 2014 *J. Phys. D: Appl. Phys.* **47** 173001
[122] Linder K, Phillips J, Qasaimeh O, Liu X, Krishna S, Bhattacharya P and Jiang J 1999 *Appl. Phys. Lett.* **74** 1355–7
[123] Kazi Z I, Egawa T, Umeno M and Jimbo T 2001 *J. Appl. Phys.* **90** 5463–8
[124] Mi Z, Bhattacharya P, Yang J and Pipe K 2005 *Electron. Lett.* **41** 742–4
[125] Mi Z, Yang J, Bhattacharya P and Huffaker D 2006 *Electron. Lett.* **42** 121–3
[126] Yang J, Bhattacharya P and Mi Z 2007 *IEEE Trans. Electron Devices* **54** 2849–55
[127] Yang J, Bhattacharya P and Wu Z 2007 *IEEE Photon. Technol. Lett.* **19** 747–9
[128] Yang J and Bhattacharya P 2008 *Opt. Express* **16** 5136–40
[129] Li L, Guimard D, Rajesh M and Arakawa Y 2008 *Appl. Phys. Lett.* **92** 263105
[130] Wang T, Liu H, Lee A, Pozzi F and Seeds A 2011 *Opt. Express* **19** 11381–6
[131] Lee A D, Jiang Q, Tang M, Zhang Y, Seeds A J and Liu H 2013 *IEEE J. Sel. Top. Quantum Electron.* **19** 1901107
[132] Wu J, Lee A, Jiang Q, Tang M, Seeds A J and Liu H 2014 *IET Optoelectron.* **8** 20–4
[133] Ward T, Sánchez A M, Tang M, Wu J, Liu H, Dunstan D J and Beanland R 2014 *J. Appl. Phys.* **116** 063508
[134] Tang M, Chen S, Wu J, Jiang Q, Dorogan V G, Benamara M, Mazur Y I, Salamo G J, Seeds A and Liu H 2014 *Opt. Express* **22** 11528–35
[135] Chen S, Tang M, Wu J, Jiang Q, Dorogan V, Benamara M, Mazur Y, Salamo G, Seeds A and Liu H 2014 *Electron. Lett.* **50** 1467–8
[136] Le Royer C 2011 *Microelectron. Eng.* **88** 1541–8
[137] Fletcher R M, Wagner D K and Ballantyne J M 1984 *Appl. Phys. Lett.* **44** 967–9
[138] Sheldon P, Yacobi B, Jones K and Dunlavy D 1985 *J. Appl. Phys.* **58** 4186–93
[139] Tanoto H, Yoon S, Ngo C, Loke W, Dohrman C, Fitzgerald E and Narayanan B 2008 *Appl. Phys. Lett.* **92** 213115
[140] Liu H, Wang T, Jiang Q, Hogg R, Tutu F, Pozzi F and Seeds A 2011 *Nat. Photon.* **5** 416–9
[141] Wang T, Lee A, Tutu F, Seeds A, Liu H, Jiang Q, Groom K and Hogg R 2012 *Appl. Phys. Lett.* **100** 052113
[142] Lee A, Jiang Q, Tang M, Seeds A and Liu H 2012 *Opt. Express* **20** 22181–7
[143] Groenert M E, Pitera A J, Ram R J and Fitzgerald E A 2003 *J. Vac. Sci. Technol.* B **21** 1064–9
[144] Liu A Y, Zhang C, Norman J, Snyder A, Lubyshev D, Fastenau J M, Liu A W, Gossard A C and Bowers J E 2014 *Appl. Phys. Lett.* **104** 041104
[145] Liu A Y, Zhang C, Snyder A, Lubyshev D, Fastenau J M, Liu A W, Gossard A C and Bowers J E 2014 *J. Vac. Sci. Technol.* B **32** 02C108
[146] Sandall I, Ng J S, David J P, Tan C H, Wang T and Liu H 2012 *Opt. Express* **20** 10446–52
[147] Sandall I, Ng J, David J, Liu H and Tan C 2013 *Semicond. Sci. Technol.* **28** 094002
[148] Chen S, Tang M, Jiang Q, Wu J, Dorogan V G, Benamara M, Mazur Y I, Salamo G J, Smowton P and Seeds A 2014 *ACS Photon.* **1** 638–42
[149] Jiang Q, Tang M, Chen S, Wu J, Seeds A and Liu H 2014 *Opt. Express* **22** 23242–8
[150] Sikorski C and Merkt U 1989 *Phys. Rev. Lett.* **62** 2164
[151] Demel T, Heitmann D, Grambow P and Ploog K 1990 *Phys. Rev. Lett.* **64** 788
[152] Tang S, Hsieh H, Tu H, You T, Lin S, Wang L and Chiang C 2010 *Thin Solid Films* **518** 7425–8
[153] Rogalski A 2003 *Prog. Quantum Electron.* **27** 59
[154] Kim S, Mohseni H, Erdtmann M, Michel E, Jelen C and Razeghi M 1998 *Appl. Phys. Lett.* **73** 963–5
[155] Hoff J, Razeghi M and Brown G J 1996 *Phys. Rev.* B **54** 10773
[156] Li S S and Tidrow M Z 1998 *Photonics China'98* pp 97–111
[157] Ryzhii V 1996 *Semicond. Sci. Technol.* **11** 759–5
[158] Urayama J, Norris T B, Singh J and Bhattacharya P 2001 *Phys. Rev. Lett.* **86** 4930
[159] Kim E, Madhukar A, Zhengmao Y and Campbell J C 2004 *Appl. Phys. Lett.* **84** 3277–9
[160] Jiang J, Tsao S, O'Sullivan T, Zhang W, Lim H, Sills T, Mi K, Razeghi M, Brown G and Tidrow M 2004 *Appl. Phys. Lett.* **84** 2166–8
[161] Chakrabarti S, Stiff-Roberts A, Su X, Bhattacharya P, Ariyawansa G and Perera A 2005 *J. Phys. D: Appl. Phys.* **38** 2135
[162] Phillips J 2002 *J. Appl. Phys.* **91** 4590
[163] Martyniuk P, Krishna S and Rogalski A 2008 *J. Appl. Phys.* **104** 034314
[164] Lin S, Tsai Y and Lee S 2001 *Appl. Phys. Lett.* **78** 2784–6
[165] Wu J, Shao D, Dorogan V G, Li A Z, Li S, Decuir E A, Manasreh M O, Wang Z M, Mazur Y I and Salamo G J 2010 *Nano Lett.* **10** 1512–16
[166] Xu S, Chua S, Mei T, Wang X, Zhang X, Karunasiri G, Fan W, Wang C, Jiang J and Wang S 1998 *Appl. Phys. Lett.* **73** 3153–5
[167] Chen S, Chen Y and Lee S 2005 *Japan. J. Appl. Phys.* **44** 6307–11
[168] Chen Z, Baklenov O, Kim E, Mukhametzhanov I, Tie J, Madhukar A, Ye Z and Campbell J 2001 *J. Appl. Phys.* **89** 4558–63
[169] Weber A, Gauthier-Lafaye O, Julien F, Brault J, Gendry M, Desieres Y and Benyattou T 1999 *Appl. Phys. Lett.* **74** 413–15
[170] Wang S, Lin S, Wu H and Lee C 2001 *Infrared Phys. Technol.* **42** 473–7
[171] Wang S, Lin S, Wu H and Lee C 2001 *Appl. Phys. Lett.* **78** 1023–5
[172] Stiff A, Krishna S, Bhattacharya P and Kennerly S 2001 *Appl. Phys. Lett.* **79** 421–3
[173] Tang S, Lin S and Lee S 2002 *IEEE Trans. Electron Devices* **49** 1341–7
[174] Lee S, Hirakawa K and Shimada Y 1999 *Appl. Phys. Lett.* **75** 1428–30
[175] Lin S, Tsai Y and Lee S 2004 *Japan. J. Appl. Phys.* **43** 167
[176] Drozdowicz-Tomsia K, Goldys E, Fu L and Jagadish C 2006 *Appl. Phys. Lett.* **89** 113510
[177] Chou S, Wu M, Lin S and Chi J 2006 *Appl. Phys. Lett.* **88** 173511
[178] Attaluri R, Annamalai S, Posani K, Stintz A and Krishna S 2006 *J. Appl. Phys.* **99** 083105
[179] Wolde S, Lao Y, Perera A U, Zhang Y, Wang T, Kim J, Schuler-Sandy T, Tian Z and Krishna S 2014 *Appl. Phys. Lett.* **105** 151107
[180] Perera A U, Lao Y, Wolde S, Zhang Y, Wang T, Kim J, Schuler-Sandy T, Tian Z and Krishna S 2014 *Infrared Phys. Technol.* (doi: 10.1016/j.infrared.2014.10.016)
[181] Kim E, Chen Z and Madhukar A 2001 *Appl. Phys. Lett.* **79** 3341–3
[182] Ye Z, Campbell J C, Chen Z, Kim E and Madhukar A 2002 *J. Appl. Phys.* **92** 7462–8
[183] Shenoi R V, Attaluri R S, Siroya A, Shao J, Sharma Y D, Stintz A, Vandervelde T E and Krishna S 2008 *J. Vac. Sci. Technol.* B **26** 1136
[184] Raghavan S, Rotella P, Stintz A, Fuchs B, Krishna S, Morath C, Cardimona D and Kennerly S 2002 *Appl. Phys. Lett.* **81** 1369–71

[185] Barve A V, Sengupta S, Kim J O, Montoya J, Klein B, Shirazi M A, Zamiri M, Sharma Y D, Adhikary S and Godoy S E 2012 *IEEE J. Quantum Electron.* **48** 1243–51
[186] Barve A, Shah S, Shao J, Vandervelde T, Shenoi R, Jang W and Krishna S 2008 *Appl. Phys. Lett.* **93** 131115
[187] Barve A, Shao J, Sharma Y D, Vandervelde T E, Sankalp K, Lee S J, Noh S K and Krishna S 2010 *IEEE J. Quantum Electron.* **46** 1105–14
[188] Barve A V, Montaya J, Sharma Y, Rotter T, Shao J, Jang W, Meesala S, Lee S J and Krishna S 2011 *Infrared Phys. Technol.* **54** 215–19
[189] Vandervelde T E and Krishna S 2010 *J. Nanosci. Nanotechnol.* **10** 1450–60
[190] Ling H, Wang S, Lee C and Lo M 2008 *Appl. Phys. Lett.* **92** 193506
[191] Huang C, Chen Y and Lee S 2012 *Appl. Phys. Lett.* **100** 043512
[192] Chakrabarti S, Adhikary S, Halder N, Aytac Y and Perera A 2011 *Appl. Phys. Lett.* **99** 181102
[193] Martí A, López N, Antolín E, Cánovas E, Luque A, Stanley C R, Farmer C D and Díaz P 2007 *Appl. Phys. Lett.* **90** 233510
[194] Wu J, Li Z, Shao D, Manasreh M O, Kunets V P, Wang Z M, Salamo G J and Weaver B D 2009 *Appl. Phys. Lett.* **94** 171102
[195] Melloch M R, Woodall J M, Harmon E S, Otsuka N, Pollak F H, Nolte D D, Feenstra R M and Lutz M A 1995 *Annu. Rev. Mater. Sci.* **25** 547–600
[196] Posani K T, Tripathi V, Annamalai S, Weisse-Bernstein N R, Krishna S, Perahia R, Crisafulli O and Painter O J 2006 *Appl. Phys. Lett.* **88** 151104
[197] Yu Z, Veronis G, Fan S and Brongersma M L 2006 *Appl. Phys. Lett.* **89** 151116
[198] Chang C, Chang H, Chen C, Tsai M, Chang Y, Lee S and Tang S 2007 *Appl. Phys. Lett.* **91** 163107
[199] Lee S C, Krishna S and Brueck S R J 2009 *Opt. Express* **17** 23160
[200] Hellström S, Chen Z, Fu Y, Qiu M, Soltanmoradi R, Wang Q and Andersson J 2010 *Appl. Phys. Lett.* **96** 231110
[201] Chang C, Sharma Y D, Kim Y, Bur J A, Shenoi R V, Krishna S, Huang D and Lin S 2010 *Nano Lett.* **10** 1704–9
[202] Lee S J, Ku Z, Barve A, Montoya J, Jang W, Brueck S R J, Sundaram M, Reisinger A, Krishna S and Noh S K 2011 *Nat. Commun.* **2** 286
[203] Lee S, Krishna S, Brueck S 2011 *IEEE Photon. Technol. Lett.* **23** 935–7
[204] Rogalski A 2006 *Opto-Electron. Rev.* **14** 84–98
[205] Henini M and Razeghi M 2002 *Handbook of Infrared Detection Technologies* (Burlington: Elsevier)
[206] Jiang L, Li S S, Liu W-S, Yeh N-T and Chyi J-I 2005 *Infrared Phys. Technol.* **46** 249–56
[207] Lin S, Lin W, Tseng C, Chao K and Mai S 2009 *Appl. Phys. Lett.* **95** 123504
[208] Kim S M and Harris J S 2004 *IEEE Photon. Technol. Lett.* **16** 2538–40
[209] Kim S M and Harris J S 2004 *Appl. Phys. Lett.* **85** 4154–6
[210] Chakrabarti S, Su X, Bhattacharya P, Ariyawansa G and Perera A U 2005 *IEEE Photon. Technol. Lett.* **17** 178–80
[211] Huang G, Yang J, Bhattacharya P, Ariyawansa G and Perera A G U 2008 *Appl. Phys. Lett.* **92** 011117
[212] Chen Z, Kim E and Madhukar A 2002 *Appl. Phys. Lett.* **80** 2490–2
[213] Ye Z, Campbell J C, Chen Z, Kim E and Madhukar A 2002 *J. Appl. Phys.* **92** 4141–3
[214] Krishna S, Raghavan S, Winckel G V, Rotella P, Stintz A, Morath C P, Le D and Kennerly S W 2003 *Appl. Phys. Lett.* **82** 2574–6
[215] Krishna S, Raghavan S, Von Winckel G, Stintz A, Ariyawansa G, Matsik S and Perera A 2003 *Appl. Phys. Lett.* **83** 2745–7
[216] Ariyawansa G, Perera A U, Raghavan G, Von Winckel G, Stintz A and Krishna S 2005 *IEEE Photon. Technol. Lett.* **17** 1064–6
[217] Jolley G, Fu L, Tan H and Jagadish C 2008 *Appl. Phys. Lett.* **92** 193507
[218] Höglund L, Holtz P, Pettersson H, Asplund C, Wang Q, Malm H, Almqvist S, Petrini E and Andersson J 2008 *Appl. Phys. Lett.* **93** 203512
[219] Krishna S, Forman D, Annamalai S, Dowd P, Varangis P, Tumolillo T Jr, Gray A, Zilko J, Sun K and Liu M 2005 *Appl. Phys. Lett.* **86** 193501
[220] Vandervelde T E, Lenz M C, Varley E, Barve A, Shao J, Shenoi R V, Ramirez D A, Jan W, Sharma Y D and Krishna S 2008 *IEEE J. Sel. Top. Quantum Electron.* **14** 1150–61
[221] Paskaleva B S, Jang W, Bender S C, Sharma Y D, Krishna S and Hayat M M 2011 *IEEE Sensors J.* **11** 1342–51
[222] Ariyawansa G, Perera A G U, Su X H, Chakrabarti S and Bhattacharya P 2007 *Infrared Phys. Technol.* **50** 156
[223] Ariyawansa G, Apalkov V, Perera A G U, Matsik S G, Huang G and Bhattacharya P 2008 *Appl. Phys. Lett.* **92** 111104
[224] Perera A, Ariyawansa G, Huang G and Bhattacharya P 2009 *Infrared Phys. Technol.* **52** 252–6
[225] Cohen N, Zussman A and Sarusi G 2001 *Infrared Phys. Technol.* **42** 391–6
[226] Touse M, Karunasiri G, Lantz K, Li H and Mei T 2005 *Appl. Phys. Lett.* **86** 093501
[227] Alves F, Amorim J, Byloos M, Liu H, Bezinger A, Buchanan M, Hanson N and Karunasiri G 2008 *J. Appl. Phys.* **103** 114515
[228] Alves F D P, Karunasiri G, Hanson N, Byloos M, Liu H C, Bezinger A and Buchanan M 2007 *Infrared Phys. Technol.* **50** 182–6
[229] Passmore B S, Wu J, Manasreh M O and Salamo G J 2007 *Appl. Phys. Lett.* **91** 233508
[230] Passmore B S, Wu J, Manasreh M O, Kunets V P, Lytvyn P M and Salamo G J 2008 *IEEE Electron. Device Lett.* **29** 224
[231] Kim J, Oh J, Hong S, Park C and Yoo T 2000 *IEEE Electron. Device Lett.* **21** 329–31
[232] Stiff A D, Krishna S, Bhattacharya P and Kennerly S W 2001 *IEEE J. Quantum Electron.* **37** 1412–19
[233] Tang S, Lin S and Lee S 2001 *Appl. Phys. Lett.* **78** 2428–30
[234] Lu X, Vaillancourt J, Meisner M J and Stintz A 2007 *J. Phys. D: Appl. Phys.* **40** 5878
[235] Chakrabarti S, Stiff-Roberts A, Bhattacharya P, Gunapala S, Bandara S, Rafol S and Kennerly S 2004 *IEEE Photon. Technol. Lett.* **16** 1361–3
[236] Jiang L, Li S S, Yeh N, Chyi J, Ross C E and Jones K S 2003 *Appl. Phys. Lett.* **82** 1986
[237] Lim H, Tsao S, Zhang W and Razeghi M 2007 *Appl. Phys. Lett.* **90** 131112
[238] Su X, Chakrabarti S, Bhattacharya P, Ariyawansa G and Perera A U 2005 *IEEE J. Quantum Electron.* **41** 974–9
[239] Bhattacharya P, Su X, Ariyawansa G and Perera A 2007 *Proc. IEEE* **95** 1828–37
[240] Shao J, Vandervelde T E, Jang W, Stintz A and Krishna S 2011 *IEEE Trans. Nanotechnol.* **10** 1010–4
[241] Ling H, Wang S, Lee C and Lo M 2009 *Infrared Phys. Technol.* **52** 281–4
[242] Luque A and Martí A 1997 *Phys. Rev. Lett.* **78** 5014
[243] Aroutiounian V, Petrosyan S, Khachatryan A and Touryan K 2001 *J. Appl. Phys.* **89** 2268
[244] Barnham K W and Duggan G 1990 *J. Appl. Phys.* **67** 3490–3
[245] Bailey C G, Forbes D V, Raffaelle R P and Hubbard S M 2011 *Proc. SPIE* **7933** 793313
[246] Luque A, Marti A and Stanley C 2012 *Nat. Photon.* **6** 146–52
[247] Nozawa T and Arakawa Y 2011 *Appl. Phys. Lett.* **98** 171108

[248] Shao Q, Balandin A A, Fedoseyev A I and Turowski M 2007 *Appl. Phys. Lett.* **91** 163503
[249] Kerestes C, Cress C D, Richards B C, Forbes D V, Lin Y, Bittner Z, Polly S J, Sharps P and Hubbard S M 2014 *IEEE J. Photovolt.* **4** 224–32
[250] Ngo C Y 2009 *J. Cryst. Growth* **311** 1885
[251] Walker A W, Theriault O, Wheeldon J F and Hinzer K 2013 *IEEE J. Photovolt.* **3** 1118–24
[252] Kerestes C, Polly S, Forbes D, Bailey C, Podell A, Spann J, Patel P, Richards B, Sharps P and Hubbard S 2014 *Prog. Photovolt. Res. Appl.* **22** 1172–9
[253] Hu W, Inoue T, Kojima O and Kita T 2010 *Appl. Phys. Lett.* **97** 193106
[254] Luque A, Martí A, López N, Antolín E, Cánovas E, Stanley C, Farmer C and Caballero L J 2005 *Appl. Phys. Lett.* **87** 083505
[255] Abouelsaood A A, Ghannam M Y and Poortmans J 2013 *Prog. Photovolt. Res. Appl.* **21** 209–16
[256] Martí A, Antolín E, Stanley C R, Farmer C D, López N, Díaz P, Cánovas E, Linares P G and Luque A 2006 *Phys. Rev. Lett.* **97** 247701
[257] Antolin E, Marti A and Luque A 2011 *Photovoltaic Specialists Conf. (PVSC), 2011 37th IEEE* 001907–12
[258] Sanguinetti S, Watanabe K, Kuroda T, Minami F, Gotoh Y and Koguchi N 2002 *J. Cryst. Growth* **242** 321–31
[259] Mellor A, Luque A, Tobías I and Martí A 2014 *Sol. Energy Mater. Sol. Cells* **130** 225–33
[260] Martí A, López N, Antolin E, Cánovas E, Stanley C, Farmer C, Cuadra L and Luque A 2006 *Thin Solid Films* **511** 638–44
[261] López N, Martí A, Luque A, Stanley C, Farmer C and Díaz P 2007 *J. Sol. Energy Eng.* **129** 319
[262] Wei G and Forrest S R 2007 *Nano Lett.* **7** 218–22
[263] Sablon K A, Little J W, Olver K A, Wang Z M, Dorogan V G, Mazur Y I, Salamo G J and Towner F J 2010 *J. Appl. Phys.* **108** 074305
[264] Oshima R, Takata A and Okada Y 2008 *Appl. Phys. Lett.* **93** 083111
[265] Laghumavarapu R B, El-Emawy M, Nuntawong N, Moscho A, Lester L F and Huffaker D L 2007 *Appl. Phys. Lett.* **91** 243115
[266] Alonso-Álvarez D *et al* 2008 *Appl. Phys. Lett.* **93** 123114
[267] Popescu V, Bester G, Hanna M C, Norman A G and Zunger A 2008 *Phys. Rev.* B **78** 205321
[268] Hubbard S M, Cress C D, Bailey C G, Raffaelle R P, Bailey S G and Wilt D M 2008 *Appl. Phys. Lett.* **92** 123512
[269] Takata A, Oshima R, Shoji Y, Akahane K and Okada Y 2010 *Photovoltaic Specialists Conf. (PVSC), 2010 35th IEEE* 001877–80
[270] Linares P, López E, Ramiro I, Datas A, Antolín E, Shoji Y, Sogabe T, Okada Y, Martí A and Luque A 2015 *Sol. Energy Mater Sol. Cells* **132** 178–82
[271] Blokhin S *et al* 2009 *Semiconductors* **43** 514–18
[272] Sugaya T, Furue S, Komaki H, Amano T, Mori M, Komori K, Niki S, Numakami O and Okano Y 2010 *Appl. Phys. Lett.* **97** 183104
[273] Sugaya T, Kamikawa Y, Furue S, Amano T, Mori M and Niki S 2011 *Sol. Energy Mater Sol. Cells* **95** 163–6
[274] Sugaya T, Numakami O, Oshima R, Furue S, Komaki H, Amano T, Matsubara K, Okano Y and Niki S 2012 *Energy Env. Sci.* **5** 6233–7
[275] Bailey C G, Forbes D V, Raffaelle R P and Hubbard S M 2011 *Appl. Phys. Lett.* **98** 163105
[276] Bailey C G, Forbes D V, Polly S J, Bittner Z S, Dai Y, Mackos C, Raffaelle R P and Hubbard S M 2012 *IEEE J. Photovolt.* **2** 269–75
[277] Zhou D, Sharma G, Thomassen S F, Reenaas T W and Fimland B O 2010 *Appl. Phys. Lett.* **96** 061913
[278] Tutu F, Wu J, Lam P, Tang M, Miyashita N, Okada Y, Wilson J, Allison R and Liu H 2013 *Appl. Phys. Lett.* **103** 043901
[279] Xu Z, Birkedal D, Juhl M and Hvam J M 2004 *Appl. Phys. Lett.* **85** 3259
[280] Kima J O, Senguptaa S, Sharmaa Y, Barvea A V, Leeb S J and Krishnaa S and Nohb S K 2012 *Proc. SPIE* **8353** 835336
[281] Lam P, Wu J, Tang M, Jiang Q, Hatch S, Beanland R, Wilson J, Allison R and Liu H 2014 *Sol. Energy Mater Sol. Cells* **126** 83–7
[282] Okada Y, Morioka T, Yoshida K, Oshima R, Shoji Y, Inoue T and Kita T 2011 *J. Appl. Phys.* **109** 024301
[283] Sablon K A, Little J W, Mitin V, Sergeev A, Vagidov N and Reinhardt K 2011 *Nano Lett.* **11** 2311–17
[284] Sablon K, Little J, Vagidov N, Li Y, Mitin V and Sergeev A 2014 *Appl. Phys. Lett.* **104** 253904
[285] Laghumavarapu R B, Moscho A, Khoshakhlagh A, El-Emawy M, Lester L F and Huffaker D L 2007 *Appl. Phys. Lett.* **90** 173125
[286] Tomić S 2013 *Appl. Phys. Lett.* **103** 072112
[287] Cuadra L, Martí A and Luque A 2002 *Physica* E **14** 162
[288] Hatch S, Wu J, Sablon K, Lam P, Tang M, Jiang Q and Liu H 2014 *Opt. Express* **22** A679–85
[289] Luque A, Linares P G, Mellor A, Andreev V and Marti A 2013 *Appl. Phys. Lett.* **103** 123901
[290] Nishikawa K, Takeda Y, Motohiro T, Sato D, Ota J, Miyashita N and Okada Y 2012 *Appl. Phys. Lett.* **100** 113105
[291] Wu J, Shao D, Li Z, Manasreh M O, Kunets V P, Wang Z M and Salamo G J 2009 *Appl. Phys. Lett.* **95** 071908
[292] Wu J, Wang Z M, Dorogan V G, Li S, Zhou Z, Li H, Lee J, Kim E S, Mazur Y I and Salamo G J 2012 *Appl. Phys. Lett.* **101** 043904
[293] Wu J, Wang Z M, Dorogan V G, Li S, Lee J, Mazur Y I, Kim E S and Salamo G J 2013 *Nanoscale Res. Lett.* **8** 1–5
[294] Scaccabarozzi A, Adorno S, Bietti S, Acciarri M and Sanguinetti S 2013 *Phys. Status Solidi (RRL)—Rapid Res. Lett.* **7** 173–6
[295] Mendes M J, Luque A, Tobías I and Martí A 2009 *Appl. Phys. Lett.* **95** 071105
[296] Atwater H A and Polman A 2010 *Nat. Mater.* **9** 205–13
[297] Wu J, Mangham S C, Reddy V R, Manasreh M O and Weaver B D 2012 *Sol. Energy Mater Sol. Cells* **102** 44–9
[298] Lu H F, Mokkapati S, Fu L, Jolley G, Tan H H and Jagadish C 2012 *Appl. Phys. Lett.* **100** 103505
[299] Sogabe T, Shoji Y, Mulder P, Schermer J, Tamayo E and Okada Y 2014 *Appl. Phys. Lett.* **105** 113904
[300] Lantratov V M, Mintairov S A, Blokhin S A, Kalyuzhnyy N A, Ledentsov N N, Maximov M V, Nadtochiy A M, Pauysov A S, Sakharov A V and Shvarts M Z 2011 *Adv. Sci. Technol.* **74** 231–6
[301] Martí A, Antolín E, Cánovas E, López N, Linares P, Luque A, Stanley C and Farmer C 2008 *Thin Solid Films* **516** 6716–22
[302] Ramiro I, Marti A, Antolin E and Luque A 2014 *IEEE J. Photovolt.* **4** 736–48
[303] Tutu F, Sellers I, Peinado M, Pastore C, Willis S, Watt A, Wang T and Liu H 2012 *J. Appl. Phys.* **111** 046101
[304] Bremner S, Pancholi A, Ghosh K, Dahal S, Liu G, Ban K, Levy M and Honsberg C 2008 *Photovoltaic Specialists Conf., 2008. PVSC'08. 33rd IEEE* pp 1–6
[305] Simmonds P J, Sun M, Laghumavarapu R B, Liang B, Norman A G, Luo J and Huffaker D L 2014 *Nanotechnology* **25** 445402
[306] Tutu F, Lam P, Wu J, Miyashita N, Okada Y, Lee K, Ekins-Daukes N, Wilson J and Liu H 2013 *Appl. Phys. Lett.* **102** 163907

[307] Wu J, Makableh Y F M, Vasan R, Manasreh M O, Liang B, Reyner C J and Huffaker D L 2012 *Appl. Phys. Lett.* **100** 051907
[308] Yang X, Wang K, Gu Y, Ni H, Wang X, Yang T and Wang Z 2013 *Sol. Energy Mater Sol. Cells* **113** 144–7
[309] Lam P, Hatch S, Wu J, Tang M, Dorogan V G, Mazur Y I, Salamo G J, Ramiro I, Seeds A and Liu H 2014 *Nano Energy* **6** 159–66
[310] Mitin V, Pipa V, Sergeev A, Dutta M and Stroscio M 2001 *Infrared Phys. Technol.* **42** 467–72
[311] Driscoll K, Bennett M F, Polly S J, Forbes D V and Hubbard S M 2014 *Appl. Phys. Lett.* **104** 023119
[312] Okada Y, Yoshida K, Shoji Y, Ogura A, García-Linares P, Martí A and Luque A 2012 *AIP Conf. Proc.* **1477** 10–3
[313] Linares P G, Martí A, Antolín E, Farmer C D, Ramiro Í, Stanley C R and Luque A 2012 *Sol. Energy Mater. Sol. Cells* **98** 240–4
[314] Linares P G, Martí A, Antolin E, Ramiro Í, López E, Farmer C D, Stanley C R and Luque A 2013 *IEEE J. Photovolt.* **3** 753–61
[315] Ramiro I, Antolín E, Steer M, Linares P, Hernandez E, Artacho I, Lopez E, Ben T, Ripalda J and Molina S I 2012 *Photovoltaic Specialists Conf. (PVSC), 2012 38th IEEE* 000652–6
[316] Luque A, Marti A, Antolin E and Garcia-Linares P 2010 *Sol. Energy Mater Sol. Cells* **94** 2032–5
[317] Sellers D, Polly S, Hubbard S and Doty M 2014 *Appl. Phys. Lett.* **104** 223903
[318] Mellor A, Luque A, Tobías I and Martí A 2012 *Appl. Phys. Lett.* **101** 133909
[319] Okada Y 2015 *Appl. Phys. Rev.* **2** 021302
[320] Tsai C, Hsu S, Lin S, Chang C, Tu L, Chen K, Lay T and Lin C 2014 *Opt. Express* **22** A359–64
[321] Sogabe T, Shoji Y, Ohba M, Yoshida K, Tamaki R, Hong H, Wu C, Kuo C, Tomić S and Okada Y 2014 *Sci. Rep.* **4** 4792
[322] Tanabe K, Guimard D, Bordel D and Arakawa Y 2012 *Appl. Phys. Lett.* **100** 193905
[323] Beattie N, Zoppi G, See P, Farrer I, Duchamp M, Morrison D, Miles R and Ritchie D 2014 *Sol. Energy Mater Sol. Cells* **130** 241–45
[324] Dahal S N, Bremner S P and Honsberg C B 2010 *Prog. Photovolt. Res. Appl.* **18** 233–9
[325] Linares P, Marti A, Antolín E and Luque A 2011 *J. Appl. Phys.* **109** 014313